Stimulation of immunity-linked genes by membrane disruption is linked to Golgi function and the ARF-1 GTPase

Matthew J. Fanelli[1], Christofer M. Welsh[1,2], Dominique S. Lui[1], Lorissa J. Smulan[3] and *Amy K. Walker[1]

[1]Program in Molecular Medicine, UMASS Chan Medical School, Worcester, MA

[2]Morningside School of Biomedical Sciences, UMASS Chan Medical School, Worcester, MA

[3]Department of Medicine, UMASS Chan Medical School, Worcester, MA

Corresponding author: amy.walker@umassmed.edu

Abstract

Immunity-linked genes (ILGs) are activated by pathogens but also may respond to imbalances in lipids. Why pathogen attack and metabolic changes both impact ILG activation is unclear. We find that ILGs are activated when membrane phosphatidylcholine ratios change in secretory organelles in *C. elegans*. RNAi targeting of the ADP-ribosylation factor ARF-1, which disrupts the Golgi, also activates ILG expression, suggesting that activation of this membrane stress response could occur outside the ER. Our data argue that ILG upregulation is a coordinated response to changes in trafficking resulting from intrinsic cues (changes in membrane lipids) or extrinsic stimulation (increased secretion during immune response). Indeed, a focused RNAi screen of ILGs uncovered defects in secretion of two GFP reporters as well as accumulation of a pathogen-responsive CUB-domain fusion protein. These results also suggests that genes shared between the classical pathogen responses and lipid stress may act to counteract stress on secretory function.

Teaser: Pathogen response genes are also activated by lipid imbalances, which we suggest occurs because both processes put stress on the secretory pathway.

34 **Introduction**

35 Cellular stress responses react to extrinsic insults by upregulating genes that defend the cell.
36 Stress responses also restore organelle function in response to intrinsic changes. Several of these
37 intrinsic stress response pathways are also linked to metabolic processes. For example,
38 overnutrition can lead to metabolic changes that induce cellular stress through an increase in
39 reactive oxygen species (*1*). Several signaling pathways play a dual role, functioning as
40 coordinators of nutrient responses as well as stress responses. For example, the nutritional
41 sensor mTORC1 can influence stress-responsive transcription (*2*). In addition, insulin signaling
42 pathways are strongly linked to stress. In addition, mutations in *daf-2*, the *Caenorhabditis*
43 *elegans* insulin receptor/insulin-like growth factor ortholog, produce highly stress-resistant
44 animals (*3*). Finally, changes in ER lipids have a profound effect on stress pathways (*4–6*).
45 Specialized ER sensors detect both the accumulation of unfolded proteins and overload of the
46 secretory pathway. These sensors then initiate gene expression programs that reduce protein
47 load or increase lipid production (*7*, *8*).
48
49 While stress responses and metabolism are clearly intertwined, the biological advantages of
50 linking these processes are less clear. For example, in a previous study, we found that RNAi-
51 mediated knockdown of two different lipid synthesis modulators, *sams-1* and *sbp-1*, caused
52 upregulation of pathogen-response genes in *C. elegans* (*9*). One of these lipid modulators,
53 *sams-1/MAT1A,* encodes an S-adenosylmethionine synthase important for phosphatidylcholine
54 (PC) production (*10*). The Troemel lab also identified *sams-1* as a regulator of the infection
55 response gene *irg-1* in an RNAi screen (*11*). The other lipid modulator identified in our previous
56 screen, *sbp-1/SREBPF1,* codes for a master transcriptional regulator of lipid synthesis genes

57 (*12*). Reduction of *sbp-1/SREBPF1* causes a decrease in total lipid stores (*13*). Notably,
58 mammalian *SREBPF1* knockdown also results in the enrichment of immunity-linked gene
59 expression in human cells (*14*). Recent studies from other labs have found that ILGs are
60 upregulated after mutation or RNAi of genes affecting PC synthesis. ILG activation was seen
61 upon disruption of *pmt-2* (*15*) or *lpin-1* in the presence of excessive glucose (*16*). These
62 immunity-linked genes were also upregulated in *skn-1* mutants, a transcriptional regulator of the
63 stress response and metabolic genes (*17*). In addition, dietary restriction results in the
64 upregulation of similar gene sets (*18*). These results together suggest that multiple types of lipid
65 imbalance seem to impact immunity-linked gene expression and that these links may be
66 conserved across species, as indicated by results in human cells cited above.
67
68 Exposure of *C. elegans* to bacterial pathogens stimulates the expression of a diverse set of
69 genes, including antimicrobial peptides, enzymes for detoxifying xenobiotics, and
70 neuromodulatory peptides to coordinate inter-organ defenses (*19–22*). However, many of the
71 genes upregulated in response to either bacteria or fungi do not fall into these clearly defensive
72 pathways (*23*) or have clear functional roles. Instead, these genes are defined by pathogen-
73 responsive expression. In order to understand why knockdown of genes acting in lipid
74 metabolism might activate genes linked to immune responses when no pathogens were present,
75 we took two approaches. First, we looked for lipid signatures that could signal this response and
76 were shared between *sams-1* and *sbp-1* by comparing lipidomics of whole animals and
77 fractioned extracts. Second, we performed a RNAi screen of genes functioning in complex lipid
78 synthesis and ER/Golgi dynamics for activation of the immunity-linked reporter, p*sysm-1::GFP*
79 (*24*). In the lipidomics studies, we found that *sams-1 and sbp-1* knockdown animals had broad

80 and distinct changes in their lipidome, but both showed lowering of PC levels in the ER/Golgi
81 fraction which we previously linked to SBP-1/SREBP1 maturation in *sams-1* animals (*25*).
82 Strengthening the links to PC, our targeted RNAi screen showed that synthesis of PC, increased
83 p*sysm-1::GFP* expression. RNAi of Golgi/ER transport regulators, including the GTPase *arf-*
84 *1/ARF1,* activated the immunity-linked reporter. Notably, some ILGs were also upregulated
85 after *arf-1*/ARF1 RNAi, suggesting that disrupting Golgi function regulates immunity-linked
86 genes. Finally, we performed a targeted screen, and found that interfering with ILGs expression
87 in *sbp-1(ep79)* animals disrupted trafficking of a secreted reporter. Taken together, our results
88 suggest that some ILGs act to balance the increased secretory load in pathogen-stimulated cells
89 or when membrane lipid balance is perturbed. While immune function is critical for host
90 defenses, immune activation in non-pathogenic conditions, such as in metabolic disease, may
91 have deleterious effects (*26*). Therefore, it is critical to define cellular roles for pathogen-
92 responsive genes. Our studies suggest that genes upregulated in response to both pathogens and
93 lipid perturbation in *C. elegans* could act to support secretory processes altered in both
94 biological contexts.
95

96 **Results**

97 ***Gene set enrichment shows upregulation of pathogen-response genes in multiple models of***
98 ***membrane dysfunction***

99 Levels of lipids within membranes are tightly monitored, and imbalances may induce cellular
100 stress pathways that regulate genes to restore lipid ratios (*8*). We previously found that *sams-1*,
101 *lpin-1,* and *sbp-1* are part of a feedback loop that responds to shifts in membrane PC levels and
102 activates immunity-linked genes (**Fig. 1A**)(*9*, *25*). In order to test why immunity-linked genes
103 are activated after disruption of lipid-synthesis regulators we first conducted a bioinformatics
104 analysis using our recently developed *C. elegans* specific gene ontology tool, WormCat 2.0.
105 This computational analysis allows combinatorial graphing of gene enrichment scores based on
106 detailed annotation of all *C. elegans* genes (*27*, *28*) and uses a nested annotation strategy
107 (Category1/Category2/Category3) to provide broader or more detailed information on genome-
108 wide datasets. The WormCat annotation strategy also includes a specialized category,
109 Unassigned, to include genes cannot be classified using our strict criteria. Genes that are
110 generally characterized are placed in UNASSIGNED at the Category 1 level in WormCat 2.0
111 ("other" in the 1.0 version), but we also use unassigned to denote genes within larger, well
112 described category whose specific roles were less clear. For example, in WormCat, genes with
113 roles in immunity are classified at the Cat1 and Cat2 level in STRESS RESPONSE: Pathogen.
114 This category is broken down into Cat3 classifications for transcriptional or signaling regulators,
115 neuropeptide-like proteins, proteins containing common antimicrobial motifs (saposin, caenacin,
116 CUB, and others).

Fanelli, et al.
Figure 1

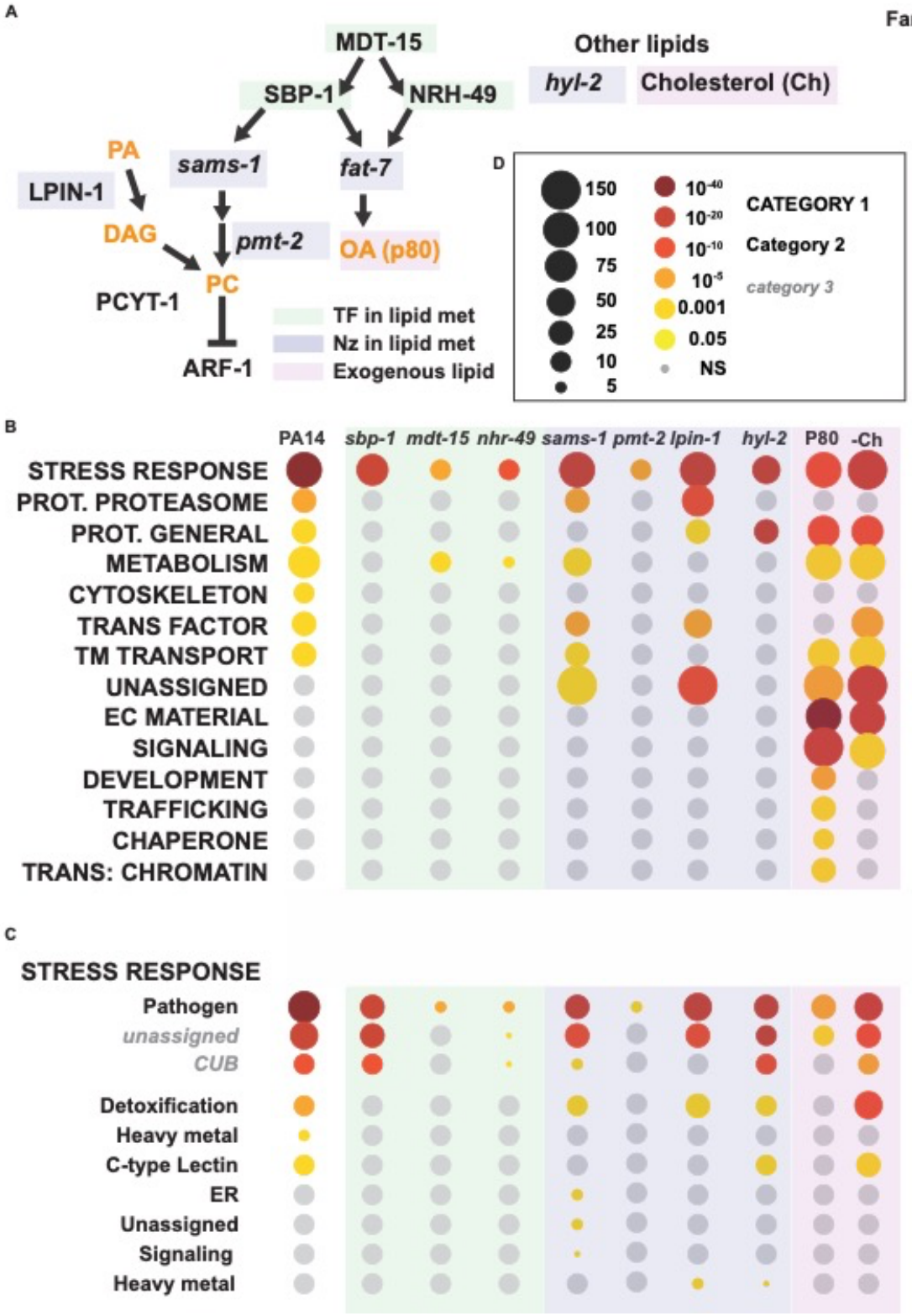

118

119 **Figure 1: Upregulation of immunity-linked genes occurs downstream of multiple types of**

120 **membrane lipid disruption. A.** Schematic diagram of lipid metabolic genes linked to immune

121 gene expression. Meta-analysis of published RNA seq data from linking lipid perturbation to

122 immune gene expression using WormCat 2.0 for Category 1 (Cat1) (**B**) and for the Category 2

123 (Cat2) level under STRESS RESPONSE (**C**).

124 Legend is in **D.**

125

126 This category also includes 97 genes upregulated during the pathogen response, but lacking
127 molecular characterization, which were designated STRESS RESPONSE: Pathogen: *unassigned*
128 (*27*, *28*). This sub-category had the highest enrichment after RNAi of *sbp-1* or *sams-1* (*27–29*),
129 suggesting that immunity linked genes upregulated after lipid unbalance could function in area
130 common to immune response and lipid stress.
131
132 In order to better characterize these ILGs, we used WormCat to perform a meta-analysis of
133 published data comparing categories enriched in genes upregulated by the pathogen PA14 (*22*)
134 with multiple models of disrupted lipogenesis (**Fig1A**). We found enrichment in
135 Category1(Cat1) STRESS RESPONSE, and more specifically in Pathogen at the Cat2 level in
136 genes upregulated after the lipogenic transcriptional regulators *sbp-1* (*9*), *mdt-15* (*30*) or *nhr-49*
137 (*31*) or enzymes acting in lipid synthesis, *sams-1* (*9*), *lpin-1* ((*16*); **DataS1**), *pmt-2* (*6*), and *hyl-2*
138 (*32*) were knocked down as well as when exogenous lipids such as P80 (oleic acid mimic) (*33*)
139 or cholesterol were added (*34*) (**Fig1B-C)**. Notably, the strongest enrichments at the Cat3 level
140 were in STRESS RESPONSE: Pathogen: *unassigned*. Genes in this category are defined by
141 solely upregulation upon pathogen exposure in *C. elegans* but do not have defined functions as
142 antimicrobial peptides or within pathogen-stimulated signaling pathways such as MAPK
143 signaling (*27*, *35*). Importantly, this class of genes is not explicitly defined by a traditional GO
144 analysis. Genes upregulated in *pmt-2(RNAi)* animals were also linked to the Lipid Bilayer Stress
145 induced Unfolded Protein Response (UPR^{LBS}), a UPR^{ER} mechanism (*6*), therefore, we compared
146 WormCat enrichment of genes increasing after tunicamycin treatment (*36*). We found that while
147 STRESS RESPONSE: Pathogen: *unassigned* genes were enriched, the category enrichment was

148 independent of the ER stress regulators *xbp-1* or *ire-1 (***FigS1A)**, suggesting potential for a
149 distinct regulatory mechanism.
150
151 We also noted that the landscape of upregulated genes was complex across other categories, with
152 STRESS RESPONSE: Detoxification enrichment scores increasing in both *sams-1* and *lpin-1* but
153 not *sbp-1* (**Fig1C**). In addition, METABOLISM: Lipid was increased after *lpin-1* RNAi
154 (**Fig1C**). These data are consistent with our previous studies showing that SBP-1 transcriptional
155 targets are upregulated in these animals (*10*). Interestingly, immunity-linked categories after
156 SREBP-1 knockdown in human melanoma cell lines (*14*). Thus, genes linked to immunity are
157 upregulated across a diverse set of lipid synthesis modulators in *C. elegans* and mammalian cells
158 and occur in the absence of pathogen stimulation.
159
160 SBP-1/SREBP1 is a basic helix-loop-helix transcription factor required to express a suite of lipid
161 metabolic genes, including *fat-7* in *C. elegans* and its ortholog SCD1 in mammals (*12*, *13*). It is
162 also necessary for the upregulation of *fat-7* in lipid-replete *sams-1(lof)* animals ((*10*) (**FigS1B**).
163 Since SBP-1 upregulates lipid synthesis genes, we tested the possibility that it directly functions
164 in ILG upregulation by using *sams-1(RNAi)* to increase the expression of multiple SBP-1 target
165 genes (*10*) and assessing the need for *sbp-1*. As we previously reported in Walker, 2011, *fat-7*
166 depends on *sbp-1* in both the control and *sams-1(RNAi)* background. However, the ILG *hpo-6* is
167 expressed at high levels when induced by reduction in *sbp-1*, *sams-1*, or in *sams-1(lof); sbp-*
168 *1(RNAi)* animals (**FigS1C**), suggesting that the effects of SBP-1 on ILG upregulation are
169 indirectly related to its function as a transcriptional regulator.
170

171 Many ILGs in *C. elegans* act downstream of signals from the p38/MAPK14 kinase PMK-1 (*22*).
172 In previous studies in *C .elegans*, we found that low PC in *sams-1(lof)* animals leads to
173 constitutive phosphorylation of PMK-1 and that ILG induction was dependent on both PC and
174 *pmk-1* (*9*). We confirmed that knockdown of *sbp-1* also induces PMK-1 phosphorylation
175 (**FigS1D**). Since ILGs can be induced in mammalian cells in response to reduction in *SREBPF1*,
176 we used siRNA to knock down the rate-limiting enzyme for PC production, *PCYT1,* in human
177 hepatoma cells (**FigS1E**). We found that p38/MAPK14 phosphorylation is induced to levels
178 similar to lipopolysaccharide (LPS). Taken together, the results suggest that upregulation of
179 ILGs in response to lipid perturbations may share regulatory link to pathogen-stimulated
180 pathways.
181
182 ***Loss of sbp-1 decreases PC levels in ER/Golgi extracts***
183 Immunity-linked gene expression and PMK-1 phosphorylation both occur after reduction in
184 *sams-1* and *sbp-1*, although these genes act at different points in lipid synthesis regulation. In
185 order to identify shared lipid signatures that might stimulate this process, we analyzed the total
186 lipidomes of these mutants by LC/MS. Because animals were lysed directly into lipid extraction
187 buffer, levels were normalized to total lipid as in (*25*). The entire lipidome was broadly altered
188 in both cases, with 27% of lipid species showing significant changes in *sams-1(RNAi)* animals
189 and 30% after *sbp-1(RNAi)* (**Fig2A, B; DataS2**). We next examined lipid levels at the class and
190 species level. As in our previous studies (*10*), *sams-1* animals showed lower PC and higher TAG
191 (Triacylglyceride) (**Fig2C**), and we also noted lower phosphatidylserine (PS) and sphingomyelin
192 (SM) levels in comparison to other lipid classes (**Fig2C, FigS2C**). TAG was lower after *sbp-1*
193 RNAi, as expected from previous studies (*37*). We also found that while reductions in PC did

194 not reach significance, PE (Phosphatidylethanolamine) increased, and Cer (Ceramide) levels
195 dropped (**Fig2C, D**). In short, *sbp-1* RNAi induces broad changes in the lipidome across
196 multiple classes of lipids.
197
198 The properties of lipid classes can be altered when distributions of acyl chains alter membrane
199 properties (*38*). We find that there are significant differences in the populations of species within
200 phospholipids (PC, PE, lyso-phosphatidylethanolamine (LPE), and phosphatidylglycerol (PG),
201 TAG, diacylglycerides (DG), and SMs after *sams-1(RNAi)*. Changes in species distribution in
202 lipid classes after *sbp-1* RNAi were limited to TAG, lyso-phosphatidylcholine (LPC), and Cer in
203 agreement with previous studies showing lower TAGs in *sbp-1(RNAi)* animals. We asked if
204 *sams-1* and *sbp-1* RNAi caused similar shifts in animals and found overlapping changes in 180
205 shared lipid species (**DataS2**). Fifty-seven of these species were decreased in both, 17 increased
206 in both, and 102 lipid species changed in opposite directions out of 1405 total lipid species
207 detected. Lipid species diverged most strongly within the TG class, with increases in *sams-*
208 *1(RNAi)* animals and decreases after *sbp-1* RNAi (**DataS2**). This agreed with total class levels.
209 For lipid species that increased in both animals, PE species were the highest, with 15 changing at
210 significant levels. Seventy-four PC species changed in both *sams-1* and *sbp-1* knockdown
211 animals, with 35 decreasing in both (**TableS3**). Finally, three SM species decreased in both
212 animals. Thus, while *sams-1* or *sbp-1* knockdown each lead to broad changes in the total
213 lipidome, relatively few overlapping species changed in both instances. Of those, PC species
214 were the best represented among lipid species that decreased upon knockdown of either *sams-1*
215 or *sbp-1* in animals.
216

Fanelli, et al.
Figure 2

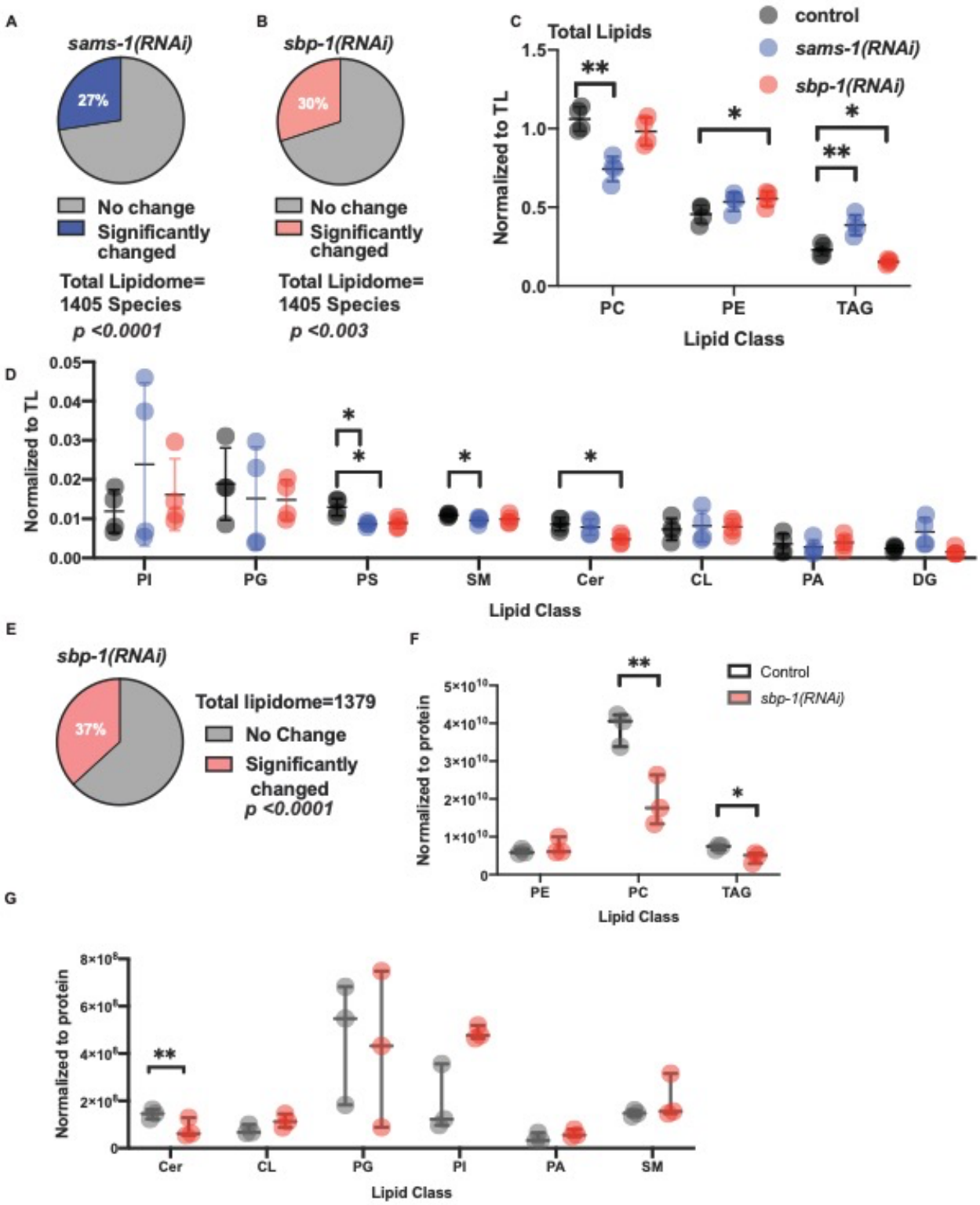

217

218

219 **Figure 2: Broad lipidomic changes in total and microsomal lipid compartments after *sams-***
220 ***1* or *sbp-1* RNAi**. LC/MS lipidomics show that nearly a third of total lipid species change after
221 *sams-1* or *sbp-1* RNAi (**A, B**). Significant changes in major lipid classes are mostly distinct in
222 *sams-1* and *sbp-1* RNAi (**C, D**). See also **Figure S1** (**B, D**) for lipid species distributions and
223 additional lipid class analysis and **Data S2** for all values. The microsomal (ER/Golgi) lipidome
224 is also broadly altered after *sbp-1 RNAi* (**E**) and shows changes in different lipid classes than in
225 the total lipidome (**F, G**). Error bars show standard deviation. Lipid class data is calculated by
226 students T-Test. See Figure S1 for lipid species distributions and additional lipid class analysis.
227

228 The total lipidome contains multiple organelles, including the plasma membrane, mitochondria,
229 nuclear membrane, and Golgi/ER. However, lipid ratios in specific organelles may be reflective
230 of particular functions; for example, we previously found that PC ratios in ER/Golgi fractions
231 were associated with activation of SBP-1 in *sams-1* and *lpin-1* animals (*25*). Therefore, we
232 performed LC/MS lipidomics on microsomes from *sbp-1(RNAi)* animals to assess lipids in the
233 ER/Golgi fraction. Because the lipidomics was performed on fractionated animals, we used total
234 protein for normalization. We found a broader fraction of the ER/Golgi lipidome was affected
235 after *sbp-1(RNAi)* than in the total lipid samples. Nearly 40% of lipid species were altered in
236 these fractions (**Fig2E; Data23**), with significant changes in species across most classes
237 (**FigS2C**). Similar to the unfractionated extracts, levels of TAG and Cer decreased in the
238 ER/Golgi (**Fig2F**). Notably, significant ER/Golgi-specific decreases occurred in PC and DG
239 (**Fig2F; FigS2D**). This demonstrates that *sbp-1(RNAi)* has distinct effects on the ER/Golgi
240 membranes and shows decreases in PC levels at the sub-compartment level, similar to *sams-1*
241 RNAi.
242
243 ***Targeted RNAi Screen Reveals roles for COP I transport in immune gene expression***
244 Low PC levels are associated with ILG expression in *sams-1* (*9*) and *pmt-2(RNAi)* animals (*6*).
245 The low PC in the ER/Golgi compartment of both *sams-1* (*25*) and *sbp-1* RNAi animals suggests
246 this could be a shared signature linked to ILG upregulation. To understand how these lipids
247 might act, we next sought to identify genes important for ILG expression. We screened for
248 upregulation of an immune reporter, p*sysm-1*::GFP (*24*), with an RNAi sub-library that targets
249 genes involved in complex lipid metabolism, lipid signaling and selected ER/Golgi transport
250 regulators. We previously used a lipid-function RNAi sub-library to identify low-PC regulators

251 of SBP-1/SREBP-1 (*25*). Notably, we constructed RNAi clones for genes not represented in the
252 Arhinger or Orfeome RNAi libraries. The resulting library includes all predicted phospholipases
253 and enzymes for synthesis of complex lipids (*25*). For the current screen, we expanded the sub-
254 library to include more genes involved in ceramide/sphingomyelin synthesis and confirmed all
255 clone identities by sequencing. Thus, this library has a broader representation of genes linked to
256 complex lipid synthesis than the commercially available RNAi libraries. p*sysm-1*::GFP is
257 strongly induced by *sbp-1(RNAi)* (**Fig3A**) and has been used by multiple labs as a robust marker
258 for immune gene induction (*18*, *39*, *40*).
259
260 In order to identify genes in lipid synthesis important for ILG upregulation, we screened this
261 library in quadruplicate in p*sysm-1*::GFP animals and identified a list of 20 candidates for
262 retesting (**Fig3B; DataS3**). Retesting to identify the strongest candidates occurred in 3 stages:
263 visual rescreening (4X), imaging of candidates from the rescreen, and qRT-PCR to assess
264 changes in GFP expression. We also included the *sbp-1* target genes *fat-5*, *fat-6,* and *fat-7* (*13*,
265 *37*) in the visual retesting. These genes are orthologs of mammalian Stearoyl CoA desaturases
266 (SCDs) (*41*) and can change membrane fluidity (*42*, *43*) or induce lipid bilayer stress by
267 changing ratios of saturated/unsaturated acyl chains within lipid classes (*6*, *15*, *44*).
268
269 Candidates from the targeted screen fell into two major groups. First, enzymes linked to PC and
270 SM synthesis were found (**Fig3C-G; FigS3A, B; DataS3**). This included two isoforms of the
271 rate-limiting enzyme for PC production, *pcyt-1,* and *sptl-1*, which initiates the first committed
272 step in sphingolipid synthesis. Thus, our genetic data supports the notion that changes in PC or
273 SMs are a shared signature linked to ILG activation in *sams-1* and *sbp-1* RNAi animals.

Fanelli, et al.
Figure 3

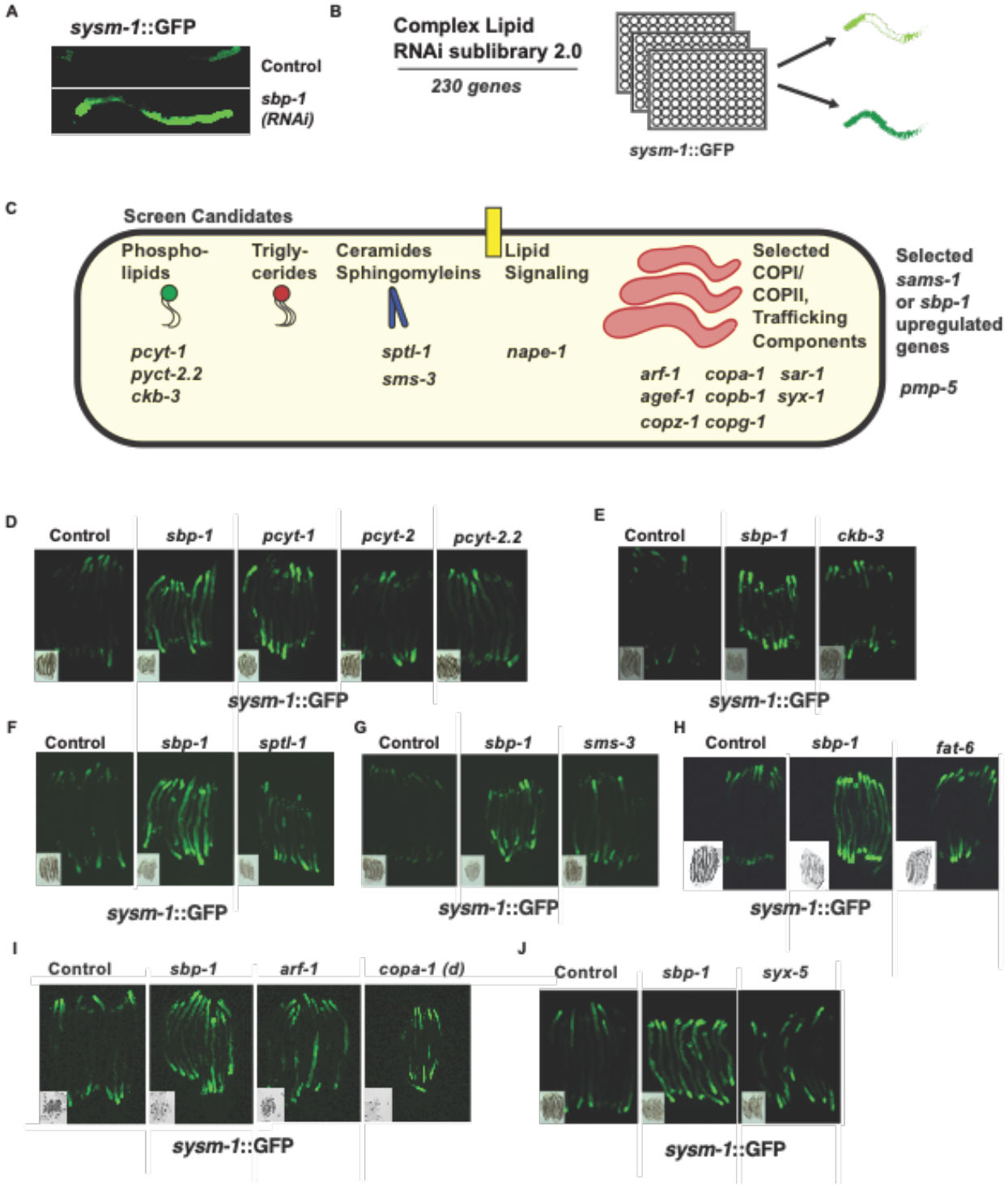

275 **Figure 3: Targeted RNAi screen reveals candidates linked to Golgi/ER trafficking and**
276 **ceramide/sphingomyelin synthesis impact immunity gene expression.** (**A**) Immune gene
277 reporter p*sysm-1*::GFP is increased after *sbp-1* RNAi. (**B**) Screen schematic. (**C**) Schematic
278 showing RNAi library coverage and screen candidates. Epifluorescence imaging showing
279 validation of reporter activity after RNAi of lipid PC synthesis genes (**D, E**), SM synthesis genes
280 (**F, G**) and the stearoyl CoA desaturase *fat6/7* (**H**). Epifluorescence images showing GFP levels
281 after RNAi of the *arf-1* GTPase or coatomer component *copa-1* or proteins acting at the Golgi
282 such as *syx-1*/Syntaxin5 (**I, J**). Because of poor larval development, bacteria for *copa-1* RNAi
283 was diluted to 1:10. Internal control for effect of *sbp-1(RNAi)* included in each panel and DIC
284 image included as an inset for each RNAi. Quantitation of images is in **Figure S4, A, B**.
285

286 Notably, *fat-5, fat-6,* or *fat-7* RNAi, which would change acyl chain saturation within each lipid
287 class, had modest effects on the p*sysm-1*::GFP immune reporter (**Fig3H, FigS3A, B; DataS3**),
288 suggesting changes in membrane fluidity downstream of these enzymes is not a major
289 contributor to the immunity-linked gene upregulation.
290
291 Second, Golgi/ER trafficking genes included four genes forming the COPI complex (which also
292 caused developmental delays) and ARF1 guanine activating factor (*agef-1*). The ARF-1
293 GTPase, a key regulator of these factors, was a false negative in the original screen, but strongly
294 activated the reporter in the rescreening. (**Fig3I**; **DataS3**). The coatomer proteins work in a
295 complex (*45*) and are required for viability (*46*). Therefore, we chose one candidate, *copa-1,* and
296 performed RNAi with diluted bacteria, allowing animals to develop fully. We found that the
297 immune activation reporter was strongly expressed in the *copa-1* knockdown (**Fig3I**).
298 Stimulation of the reporter after the loss of multiple parts of the COP I machinery and its key
299 regulator *arf-1* strongly argues that ER/Golgi dynamics signal to induce immunity-linked genes.
300 The p*sysm-1*::GFP reporter represents a single gene in the immune response program. To more
301 broadly survey ILGs in our screen validation, we used qRT-PCR with primers specific to *irg-1,*
302 *irg-2,* and *hpo-6*, and found robust activation of each of our candidate reporters after knockdown
303 of *arf-1* or *copa-1*, but more modest effects with the SM genes or SCDs (**FigS4C-H),** implicating
304 ARF1 and Golgi function in ILG activation.
305
306 ***Disruption of ER/Golgi activates immunity-linked genes***
307 Cycling of the ARF1 GTPase requires interaction with the Golgi membrane (*45*). Alteration of
308 membrane lipid ratios can affect interactions with ARF1 regulatory proteins, limiting GTPase

309 cycling and blocking ARF1 activity (*25*, *47*). We previously linked changes in PC levels in
310 *sams-1* microsomes to the inactivation of ARF-1, which drove proteolytic processing of SBP-
311 1/SREBP-1 (*25*). Therefore, we reasoned that multiple modes of membrane lipid disruption
312 could signal secretory stress through ARF-1 and activate ILGs. The upregulation of *sysm-1* and
313 other immune genes after *arf-1* RNAi prompted us to examine genome-wide changes in the
314 transcriptome that could occur in response to the loss of ARF-1 function. Using RNA-seq, we
315 found that 705 genes were significantly upregulated after *arf-1* RNAi (**Fig4A, DataS4**) and that
316 40% of genes were also upregulated in *sams-1* or *sbp-1* RNAi animals (**Fig4B**). Downregulated
317 genes in *sams-1, sbp-1,* or *arf-1* animals had low levels of overlap (**Fig4C**). WormCat gene set
318 enrichment shows that STRESS RESPONSE: Pathogen: *Other* gene sets are significantly
319 upregulated in *arf-1(RNAi)* animals as they are after *sbp-1, sams-1,* or *lpin-1* RNAi (**Fig4D-F**).
320 Next, we examined WormCat enrichment within the genes that were shared between these three
321 RNAi sets and found that shared genes retained strong enrichment for STRESS RESPONSE:
322 Pathogen (**Fig4D-F**). Thus, *arf-1* GTPase knockdown causes similar or overlapping effects in
323 immune gene expression to those seen after broad lipid disruption by *sbp-1* RNAi.
324
325 In order to study the localization of ARF-1, we obtained a strain where endogenous ARF-1 is C-
326 terminally tagged with mCherry by CRISPR (WAL10). Next, we asked if ARF-1 localization
327 was altered in *sbp-1(RNAi)* animals by examining expression in the ARF-1::mCherry animals.
328 In intestinal cells, ARF-1::mCherry formed a punctate pattern (**Fig4G-H**) characteristic of the
329 Golgi ministacks occurring in *C. elegans* cells (*48*) and which localize adjacent to a Golgi
330 marker, MANS::GFP (*49*), expressed in the intestine. MANS::GFP is a fusion of *aman-2* (alpha-
331 mannosidase, a conserved Golgi specific protein) and marks the mini-Golgi stacks characteristic

of these

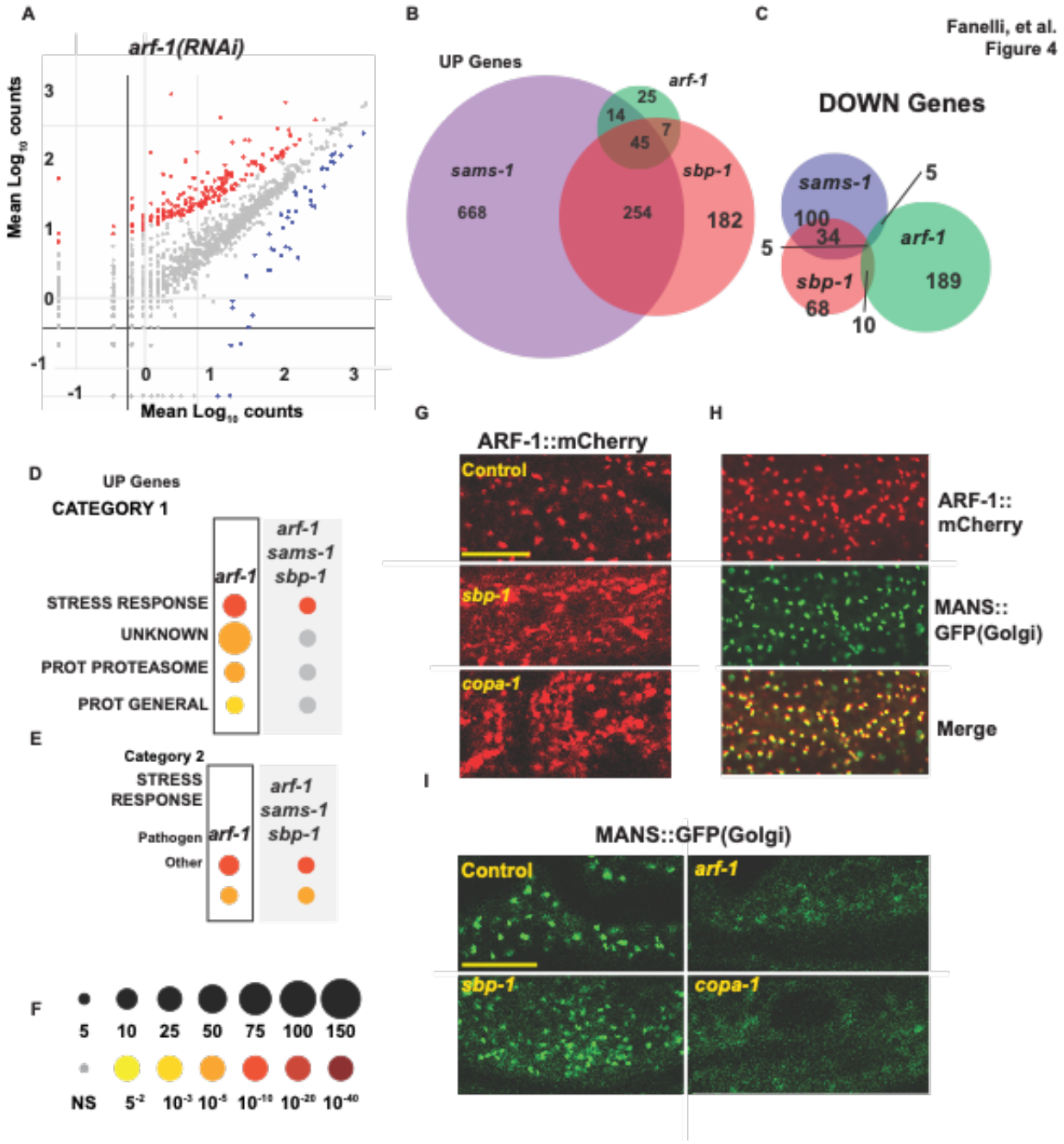
Fanelli, et al.
Figure 4
A
arf-1(RNAi)
Mean Log10 counts
Mean Log10 counts
B
UP Genes
arf-1
sams-1
sbp-1
668
25
14
7
45
254
182
C
DOWN Genes
sams-1
arf-1
sbp-1
100
34
68
189
5
5
10
D
UP Genes
CATEGORY 1
arf-1
arf-1
sams-1
sbp-1
STRESS RESPONSE
UNKNOWN
PROT PROTEASOME
PROT GENERAL
E
Category 2
STRESS RESPONSE
Pathogen
Other
arf-1
arf-1
sams-1
sbp-1
F
5 10 25 50 75 100 150
NS 5-2 10-3 10-5 10-10 10-20 10-40
G
ARF-1::mCherry
Control
sbp-1
copa-1
H
ARF-1::
mCherry
MANS::
GFP(Golgi)
Merge
I
MANS::GFP(Golgi)
Control
arf-1
sbp-1
copa-1

334 **Figure 4: Disruption of Golgi/ER trafficking increases expression of immunity-related**
335 **genes. A.** Scatter plot shows changes in gene expression after *arf-1* RNAi. Venn diagrams
336 showing limited overlap of up- (**B**) or downregulated (**C**) genes after *sbp-1, sams-1* or *arf-1*
337 RNAi. WormCat gene set enrichment chart shows an increase in stress response and pathogen
338 linked genes in Category1 (**D**) and Category2 levels (**E**). Legend is in **F**. **G.** Confocal
339 projections of endogenously tagged ARF-1::mCherry reveal that that Golgi-like pattern is
340 disrupted after *sbp-1* RNAi and quantitation in **Figure S5A**. **H**. Confocal images of intestinal
341 cells from ARF-1::mCherry; ges-1::MANS-1::GFP animals. Scale bar is 10 microns. **I**.
342 Confocal projections of the *C. elegans* Golgi marker MANS::GFP (*49*) in Control, *sbp-1, arf-1,*
343 and *copa-1 (1:10)* RNAi intestines with quantitation of puncta intensity and number in **Figure**
344 **S5B, C**. Scale bar is 10 microns. Significance is determined by the Mann-Whitney test.
345

346 of *C. elegans* (*50*). This suggests that, as in other eukaryotes, *C. elegans* ARF-1 acts at the
347 Golgi apparatus. Strikingly, ARF-1::mCherry appeared to form larger, more irregular punctae in
348 *sbp-1(RNAi)* animals as well as having additional diffuse localization, similar to patterns seen
349 with RNAi of the coatomer protein COPA-1 (**Fig4C**). This suggests that ARF-1 functions at the
350 Golgi are altered in *sbp-1(RNAi)* animals.
351
352 Loss of human ARF1 or blocking ARF1 cycling with the fungal toxin Brefeldin A disrupts Golgi
353 integrity (*51*). In addition, our previous studies found that lowering PC levels through RNAi of
354 *sams-1* or knockdown of *PCYT1* (the rate-limiting enzyme for PC production) in mammalian
355 cells blocked ARF1 GTPase activity and disrupted Golgi structure (*10*, *25*). Because PC levels
356 in *sbp-1(RNAi)* ER/Golgi fractions decreased (**Fig2C**) and ARF-1::mCherry was mis-localized,
357 we next examined Golgi structure after *sbp-1(RNAi)* in animals where MANS::GFP was driven
358 by an intestinal reporter (*49*). Consistent with previous studies (*52*, *53*), knockdown of *arf-1*
359 dramatically shifts the Golgi puncta to diffuse localization across the cytoplasm (**Fig4I; Fig**
360 **S5A**). *copa-1* RNAi also diminished Golgi stacks along with altering ARF-1::mCherry
361 localization. *sbp-1* knockdown affects Golgi structure, but results in a different pattern, in which
362 Golgi stacks are smaller and more numerous with increases in diffuse cytoplasmic localization
363 (**Fig4I, Fig5A**). We also examined MANS::GFP patterns in other candidates from our screen
364 and noted that like *arf-1*, *copa-1* and *sar-1* were required for MANS-1::GFP puncta (**FigS5B, C**),
365 as expected for core constituents of COP I and COP II transport. Contributors to PC synthesis
366 also broadly abrogated MANS::GFP puncta, however, change in fatty acid desaturation, which
367 induces UPR^{LBS} (*6*), caused a slight increase in MANS::GFP puncta intensity, suggesting that
368 membrane stress initiated by Golgi misfunction has separable defects. Our screen candidates

369 also included genes from ceramide synthesis, which can also affect membrane function (*54*).
370 Notably, *sptl-1(RNAi)* did not noticeably alter Golgi marked by MANS::GFP and ARF-
371 1::mCherry puncta were visible (**FigS5A, D**), suggesting that *sptl-1* knockdown may mediate
372 effects on immune genes through distinct cellular membranes. Taken together, we find that
373 ARF-1 activity (*25*) and localization (this study) can be affected by *sams-1* or *sbp-1* RNAi and
374 that targeting *arf-1* or the coatomer components can activate ILGs. Thus, blocking or limiting
375 ARF-1 function at the Golgi may be part of the signal to activate these genes.
376
377 ***Immunity-linked gene upregulation in models of trafficking dysfunction***
378 The Golgi apparatus accepts proteins from the ER that are destined for secretion, processing
379 them by glycosylation before secretory vesicles are loaded (*55*). Stimulation of the innate
380 immune system may significantly impact trafficking load, as antimicrobial peptides are shuttled
381 through the membrane trafficking system (*56*). Indeed, activation of the ER stress response has
382 been noted in multiple systems when large numbers of proteins need to be produced and secreted
383 (*57*). Interestingly, previous data suggest that induction of membrane stress may also be a sensor
384 of infection (*58*). Based on work by the Ewbank lab, they also suggested that some pathogen-
385 response genes act to support the trafficking of antimicrobial peptides (AMPs) (*58*, *59*). We
386 noted that the immunity-linked genes upregulated at low PC are largely outside of the
387 antimicrobial categories and are comprised of gene sets defined by their shared expression upon
388 pathogen exposure rather than function (*23*, *27*). We hypothesized that some of these genes
389 might be responding to direct stress on the trafficking system.
390

391 To explore this idea, we turned to two commonly used systems for studying trafficking in *C.*
392 *elegans*, comparing ILG gene expression in strains with increasing copy number of
393 VIT-2::GFP (*60*) and visualization of trafficking in both VIT-2::GFP and *myo-3*::ssGFP (*61*).
394 *vit-2* is a vitellogenin produced and secreted from intestinal cells then taken up by the germline
395 (*62*). *myo-3*::ssGFP has a signal sequence on the fluorophore and is expressed in body wall
396 muscle (*61*). First, we used WormCat to examine category enrichment data from two published
397 studies examining genome-wide mRNA expression patterns when *vit-2* is overexpressed or
398 misregulated, placing stress on the secretory system. The Blackwell lab showed that germline-
399 less *glp-1* mutants exhibit *vit-2*::GFP buildup near its production site in the intestines (*63*).
400 WormCat analysis of their RNA seq data found strong enrichment patterns in STRESS
401 RESPONSE: Pathogen. (**Fig5A**, **C; DataS4**). Next, we used WormCat to examine RNA-seq
402 data from VIT-2::GFP (*64*) overexpressing animals produced by the Aballay group and also
403 found increases in the Stress Response category enrichment (**Fig5B, C; DataS4).** As two
404 models sharing VIT-2::GFP secretory overload show increases in STRESS RESPONSE:
405 Pathogen genes, we sought to directly test this model by comparing ILG expression in two
406 strains with a differing copy number of *vit-2*; RT130, made by microparticle bombardment and
407 containing the GFP array in addition to wild type copies (*65*) and BCN9071 which is a CRISPR-
408 generated allele integrated into the endogenous locus (*66*) (**Fig5D-F**). While VIT-2::GFP
409 intestinal puncta appeared similar in control conditions, RNAi of *arf-1* produced larger
410 aggregates in RT130 (**Fig5D**), suggesting that this strain is sensitized to stress in the secretory
411 system. Strikingly, expression of ILGs increase with VIT-2::GFP copy number (**Fig5G-J**),
412 demonstrating that ILG expression can be induced in the absence of pathogens by altering
413 increasing expression of proteins destined for the secretory pathway.

Fanelli, et al.
Figure 5

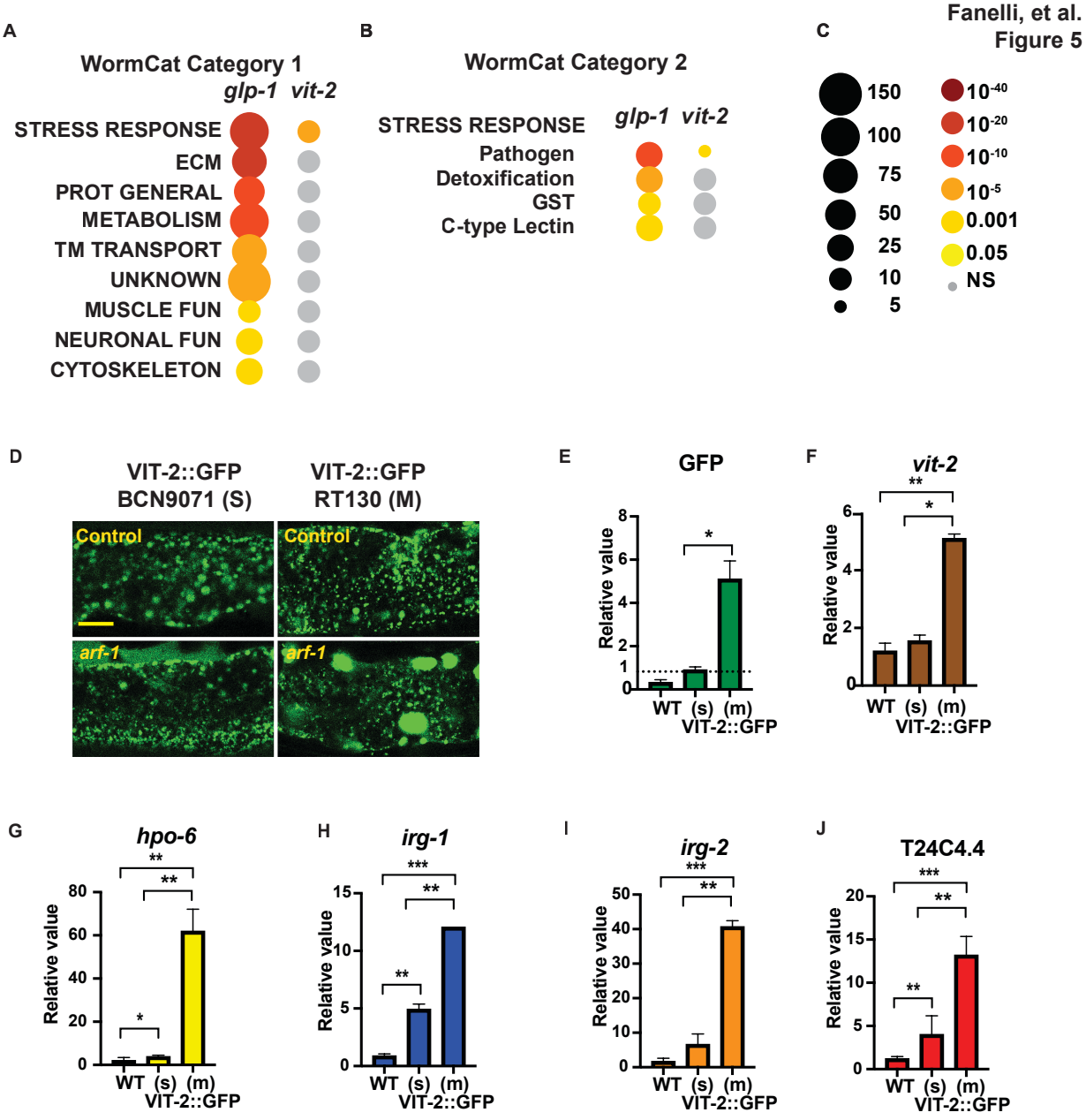

414

415 **Figure 5: Immunity-linked gene expression is linked to trafficking disruption.** WormCat
416 gene enrichment of upregulated genes from *glp-1*(AA2735) (*63*) and *vit-2(ac3)* compared to
417 SJ4005 (*64*) for Category 1 (**A**) and Category 2 (**B**). Legend is in **C**. **D.** Confocal projections of
418 *C. elegans* intestinal cells expressing *vit-2*::GFP (RT130) or *vit-2*::GFP (*BCN9701*) in wild type
419 or *arf-1(RNAi)* animals. qRT-PCR comparing gene expression in wild type, single copy *vit-*
420 *2::GFP* (BCN9071, s) or multi copy (RT130, m) animals. **E** and **F** show increase in GFP or *vit-*
421 *2*. Immune response genes are shown in **F-J**. Significance is determined by Students T Test.
422
423

424 **Knockdown of STRESS RESPONSE: Pathogen genes disrupt a trafficking reporter**

425 We found that ILGs become upregulated in the absence of pathogen response when lipid levels
426 become unbalanced, ARF-1 functions are compromised, or when production of secreted proteins
427 increases. This prompted us to ask if some ILGs might function as part of a response to help
428 stimulate passage through the secretory pathway when trafficking load is high, as when pathogen
429 responses drive antimicrobial protein production, or when the structures of the secretory system
430 are compromised. As a pilot experiment, we focused on one of the most strongly upregulated
431 genes, *hpo-6*, which is not present in any of the commercially available RNAi libraries. To study
432 its function more closely in this context, we made a cDNA construct to allow RNAi in VIT-
433 2::GFP RT130 in wild type and *sams-1(lof)* animals (*9*). *hpo-6* was originally identified in a
434 screen for genes whose loss increased sensitivity to a pore-forming toxin (*67*). It has a
435 glycoprotein domain and may occur in membrane rafts (*68*), but has no apparent homology to
436 human proteins. *hpo-6(RNAi)* causes a slight increase in VIT-2::GFP in wild-type animals
437 (**FigS6A**). However, in the low PC *sams-1(lof)* background, VIT-2::GFP pooling and
438 aggregation suggested a broad effect on trafficking patterns. Yolk in *C. elegans* consists of both
439 lipids and proteins (*69*). Because low lipid levels in *sbp-1(RNAi)* animals makes results with
440 VIT-2::GFP difficult to interpret, we used the *myo-3*::ssGFP reporter model (*61*), which
441 expresses and secretes GFP in body wall muscle cells.

442

443 We conducted a small scale screen of 19 other STRESS RESPONSE: Pathogen: unassigned
444 genes on secretion in *myo-3*::ssGFP and the sensitized *sbp-1(ep79)*; *myo-3::GFP* backgrounds,
445 imaging body wall muscle cells in triplicate and manually scoring aggregation in blinded

446 samples (**Fig6A**). *hpo-6* and two other candidate genes, *irg-2* and ZK6.11/*irg-8* were validated
447 by confocal imaging, blinded visual scoring and quantitation of puncta size and number with
448 Cell Profiler (*70*). We found that as in *arf-1* RNAi, reduction in *hpo-6, irg-2* and *irg-8*/ZK6.11
449 increased puncta size (**Fig6B-D; FigS6; D-E**), with related decrease in aggregate number in both
450 wild type and the *sbp-1(ep79)* background, reflecting aggregation and disruption of normal
451 secretory processes.
452
453 Many of the STRESS RESPONSE: Pathogen genes are expressed in the intestine; therefore, we
454 also examined a ssGFP expressed under the *glo-1* promoter (*71*) (**Fig6E**). Using epifluorescence
455 imaging, we found that intestinal ssGFP accumulated after RNAi of *sbp-1, arf-1, hpo-6, irg-2*
456 and *irg-8* (**Fig6F, G**). Confocal imaging shows that ssGFP puncta aggregate in the intestine of
457 *sbp-1(RNAi)*animals, as in muscle tissue and that this also occurs with *hpo-6* RNAi (**Fig6G, H**).
458 Thus, in a variety of cell types, we find that interference with *sbp-1*, or candidate STRESS
459 RESPONSE: Pathogen genes, causes aggregation and pooling of ssGFP in the absence of
460 pathogen stimulation, suggesting a role in secretory processes.
461

Fanelli, et al.
Figure 6

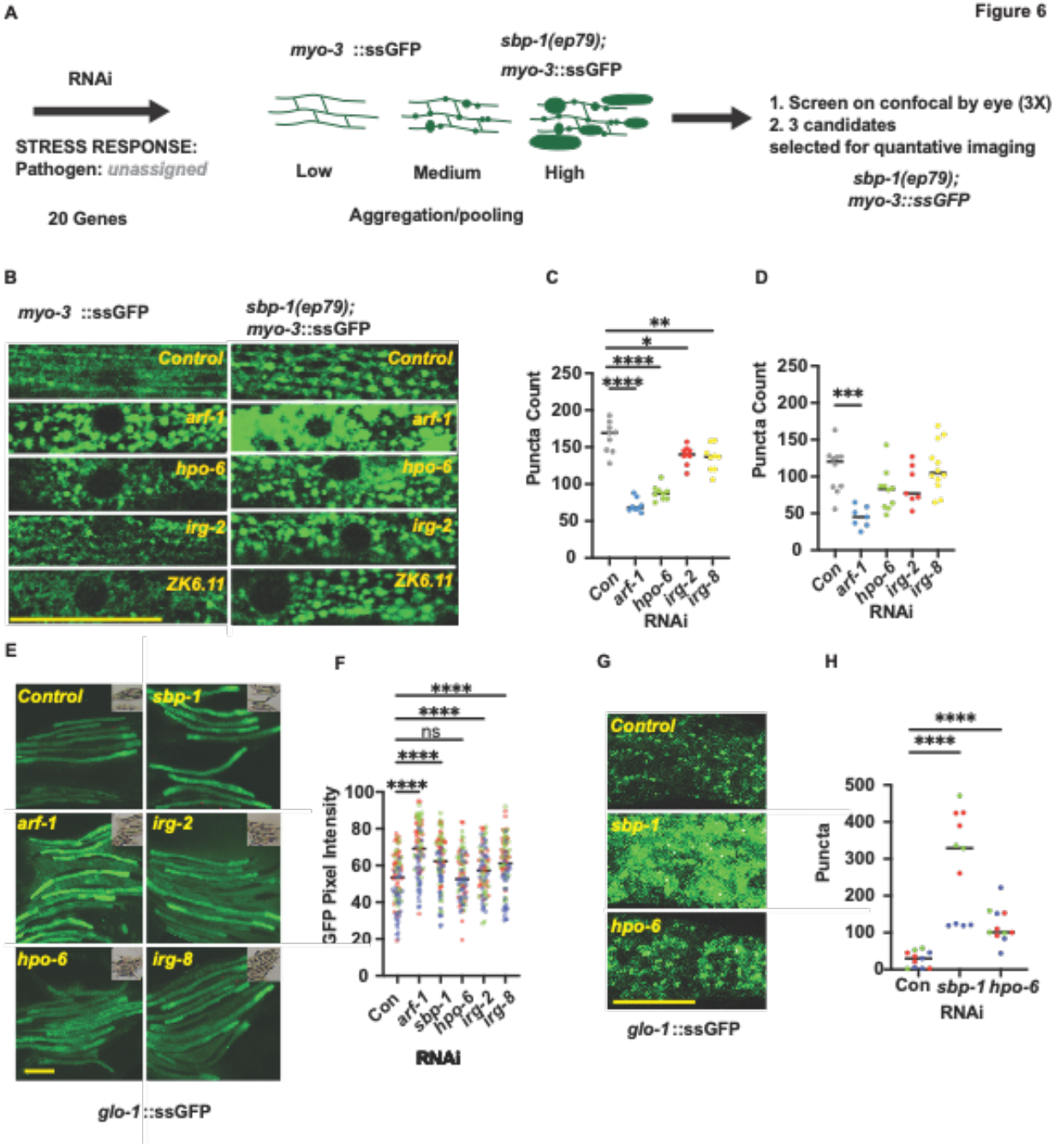

462

463 **Figure 6: ILG loss can enhance aggregation of secreted proteins.**

464 **A.** Schematic diagram of small-scale screen of STRESS RESPONSE: Pathogen: *other* genes for
465 aggregation of a secreted reporter in body wall muscle (*myo-3*::ssGFP). Confocal projections of
466 ssGFP in body wall muscle in control or the *sbp-1(ep79)* background (**B**). Quantification of
467 three independent replicates by Cell Profiler determining number of puncta (**C, D**) and puncta
468 area (**Figure S6D, E**). **E**. Epifluorescence images of ssGFP expressed from an intestinal
469 reporter with DIC images as insets. Quantitation of pixel intensity with ImageJ is in **F**.
470 Confocal projections showing ssGFP aggregation in **G**, with puncta quantitation by Cell Profiler
471 in **H**. Significance is determined by the Mann-Whitney test.

472

473

474

475 **Knockdown of STRESS RESPONSE: Pathogen genes affects an endogenous PA14**
476 **stimulated peptide**
477 The secretory pathway carries out many basal functions and must increase capacity during
478 stresses which require increases in protein production, such as pathogen challenge. The ER
479 stress pathway plays a key role during this increase (*72*, *73*) and our results suggest that
480 alterations in the Golgi may also be sensed and result in upregulation of ILGs. Our studies
481 ssGFP reporters allowed isolation of effects of lipid imbalances on basal secretory processes
482 from the complex response to pathogens. However, ILGs are defined by high level expression
483 upon pathogen exposure and could also affect secretion of antimicrobial peptides (AMPs) or
484 other defensive molecules. *C. elegans* contains a large number of proteins with domains
485 common to AMPs such as ShKT, Sushi and CUB domains (*74*). In order to test effects of the
486 ILGs on an endogenous secreted protein in the pathogen response, we selected C32H11.9/*cld-1*
487 (cub-like domain 1). In our previous RNA seq experiments, it was the highest upregulated gene
488 after PA14 exposures (**Fig7A**) and was also strongly induced during other early timepoints (*22*),
489 but not induced by lipid imbalances in *sbp-1(RNAi)* animals (**Fig7B**). It contains a signal
490 sequence, suggesting that is secreted and a CUB domain (**Fig7C**). We obtained an allele with
491 GFP fused to the C terminus of *cld-1*/C32H11.6 using CRISPR
492 (PHX2081(C32H11.6::GFP(*sybIS7080*)), which accumulated in intestine after PA14 exposure
493 (**Fig7D**), consistent with disruption with secretion. Notably, RNAi of *sbp-1* disrupted CLD-
494 1::GFP production, causing increases total levels, aggregation and accumulation in the
495 pseudocoelom, consistent with defects in secretory processes resulting from lipid imbalances
496 (**Fig7D**). Knockdown of with *arf-1* also produced similar effects, strengthening these links.
497 Interference with *hpo-6*, a candidate ILG, also caused accumulation and aggregation of CLD-

498 1::GFP during PA14 exposure, suggesting that some ILG genes act to support secretory function

499 during stress, which may be initiated by lipid imbalances or pathogen exposure.

500

501

502

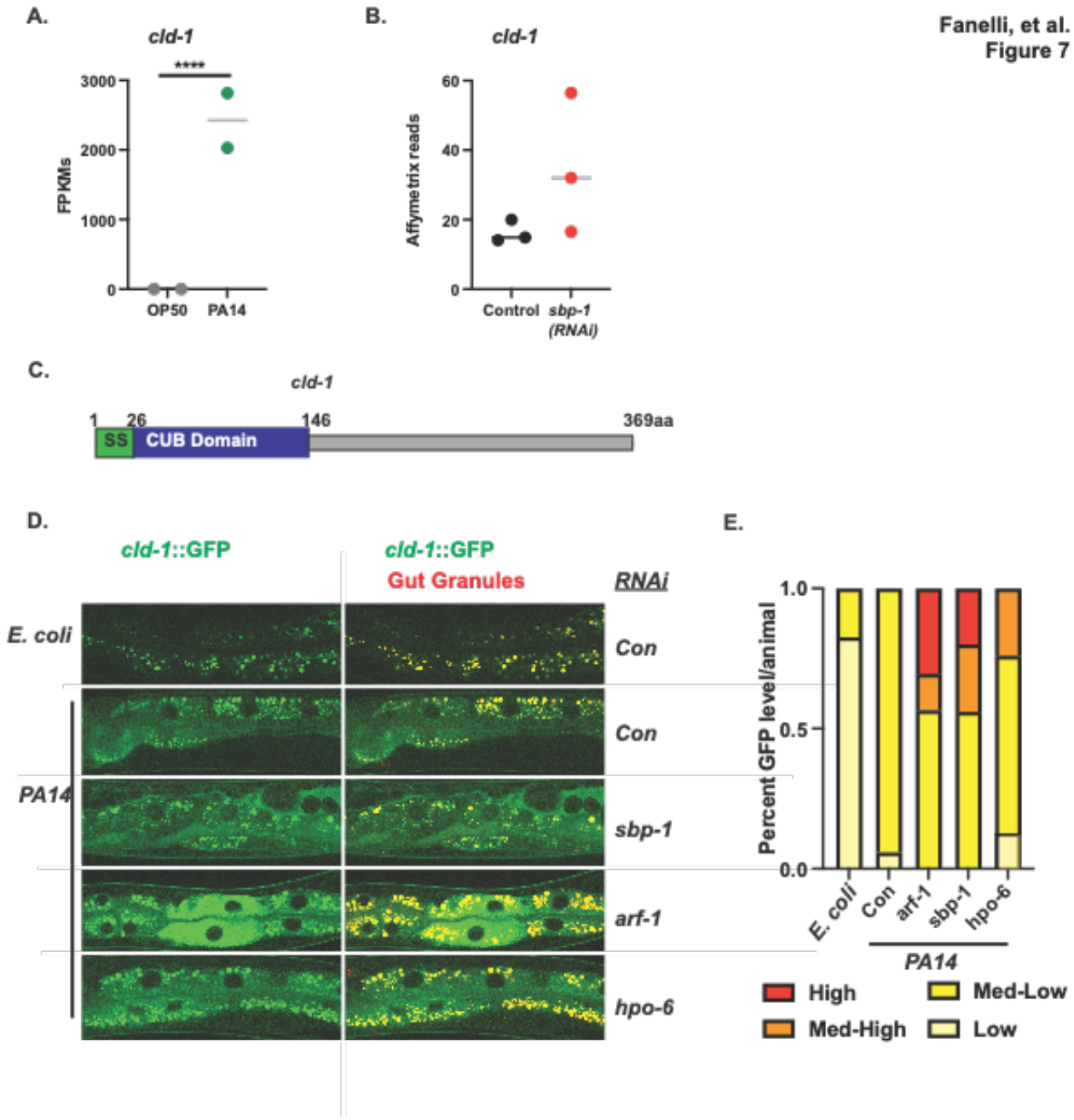
Fanelli, et al.
Figure 7
A.
cld-1
****
FPKMs
3000
2000
1000
0
OP50
PA14
B.
cld-1
Affymetrix reads
60
40
20
0
Control
sbp-1 (RNAi)
C.
cld-1
1
26
146
369aa
SS
CUB Domain
D.
cld-1::GFP
cld-1::GFP
Gut Granules
RNAi
E. coli
PA14
Con
Con
sbp-1
arf-1
hpo-6
E.
Percent GFP level/animal
1.0
0.5
0.0
E. coli
Con
arf-1
sbp-1
hpo-6
PA14
High
Med-Low
Med-High
Low

503

504 **Figure 7: ILG loss can enhance intestinal accumulation of a Pseudomonas-induced CUB**

505 **domain peptide.**

506 Expression levels of C32H9.11 in response to Pseudomonas aeruginosa (PA14) from Ding, et al.

507 2018 (**A**) or after *sbp-1* RNAi from Ding, et al. 2015 (**B**). **C.** Domain structure of C32H11.9

508 showing signal sequence and CUB domain. **D.** Spinning disc confocal micrographs showing

509 intestinal accumulation of *cld-1*/C32H11.9::GFP in response to PA14 after *sbp-1*, *arf-1* or ILG

510 RNAi taken at 488mn. Gut granules are shown with an overlay of a micrograph of the same

511 section from taken at 564nm. Quantitation is in **E**.

512

513 **Discussion**

514 Pathogen elicited gene expression programs are part of a specialized stress response where
515 specific sets of antimicrobial peptides are produced, then secreted in response to pathogens. This
516 type of innate immune response initiates as pathogens are recognized by interaction with cellular
517 proteins or cellular processes are disturbed (*75*). In *C. elegans*, evidence for microbe/pathogen
518 associated molecular patterns (MAMPS/PAMPS) has been less clear, however, surveillance of
519 cellular processes such as translation (*11*), initiating the unfolded protein response or impacting
520 lipid bilayer function activates pathogen responsive signaling and transcription of ILGs (*9*, *15*,
521 *16*, *34*). While some studies have suggested changing levels of specific lipids can prime
522 pathogen responses (*34*), lipid perturbations activating pathogen-responsive gene expression do
523 not necessarily confer pathogen resistance (*9*), and ILG expression levels may be much lower
524 than what occurs in a pathogen response. Links between membrane lipid levels and immune
525 gene activation also occur in other organisms. In *Drosophila*, synthesis of PC is critical to
526 immune function, balancing stored lipids with need to maintain membranes for secretory
527 processes (*76*). In mammals, interference with a master transcriptional regulator of lipid
528 biosynthetic enzymes, *sbp-1/SREBP-1* activates a gene expression program shared with pathogen
529 stress in both *C. elegans* and mammals (*14*). This raises the larger the question of why ILG
530 expression increases when membrane lipids are unbalanced in the absence of pathogens.
531

532 Membrane lipids form the organelles of the secretory system, which can sense changes in protein
533 homeostasis or lipids levels and elicit gene expression programs when stressed. Multiple well-
534 studied pathways are linked to changes in proteostasis or lipid levels within the ER (*57*). These
535 processes are orchestrated by ER-intrinsic proteins that sense changes in protein folding or

536 alterations in the lipid bilayer (*6*, *8*, *15*, *77*). These ER-linked events are also important during
537 pathogen exposure in *C. elegans*; changes in ribosomal function at the ER have a well-defined
538 impact on pathogen responses (*11*, *78*) and pathogen responses depend on ER stress pathways to
539 protect this organelle from the demands of the immune response (*73*, *79*). Interestingly, the Lee
540 lab also found that ILGs are upregulated when trafficking is inhibited through blocking
541 glycosylation in the ER (*80*). In addition, pathogen-responses require an intact ER stress
542 pathway to allow adjustment to the increased trafficking load (*58*, *73*), as antimicrobial peptides
543 are produced in mass in the ER, sent in lipid vesicles to the Golgi, where many are glycosylated
544 and then packaged into lipid vesicles for secretion (*81*). For example, the *C. elegans* genome
545 contains more than 300 genes that are produced in response to specific pathogens and which
546 share similarity to known antimicrobial effectors (*82*). However, many of the genes in the *C.*
547 *elegans* innate immune response do not have obvious similarity to antimicrobial effectors and are
548 defined solely as being responsive pathogens (*27*, *83*). It is this class that are largely shared
549 between pathogen-induced and membrane stress-induced stress programs. Several lines of
550 evidence prompted us to hypothesize that some of these genes might be part of a response linked
551 to stress in membranes of the secretory pathway rather than a direct response to an extrinsic
552 pathogen. First, the involvement of secretory organs was implicated by alterations in PC ratios
553 in the ER/Golgi in both *sams-1* and *sbp-1* RNAi lipidomes. Second, our targeted RNAi screen
554 for regulators of p*sysm-1::GFP* identified the *arf-1* GTPase and coatomer proteins, which are
555 critical Golgi/ER transport. Importantly, knockdown of *arf-1* was sufficient to induce ILG
556 upregulation. Strengthening this link between disruption of lipid levels and ARF-1 function, we
557 also found *sbp-1* RNAi altered ARF-1::mCherry localization and Golgi morphology.
558

559 Other organelles in the secretory pathway, such as the Golgi, have their own stress sensors and
560 response pathways (*84*), some of which act by impacting the ARF1 GTPase (*85*). ARF-1 is a
561 critical regulator of trafficking, coordinating retrograde traffic from the Golgi to the ER and
562 regulating secretory function in the trans-Golgi (*86*). Cycling of ARF-1 GTPases depends on
563 membrane localization of the ARF GTPase, GEF (Guanine exchange factor), and GAP (GTPase
564 activating protein) (*86*). We previously found that knockdown of PC synthesis enzymes blocked
565 ARF1 cycling and limited membrane association of the ARF GEF GBF1 in cultured human cells
566 (*25*). This suggests low PC levels affect ARF1 activity by limiting the ability of the GTPase,
567 GEF, and GAP to associate at the Golgi membrane and initiate GDP-GTP cycling. However, PC
568 could be linked to ARF1 through other mechanisms. ARF1 and phospholipase D (PLD) function
569 have been linked by multiple labs (*87*). PLD cleaves PC molecules to produce choline and
570 phosphatidic acid, which in turn stimulates vesicle formation (*88*). This regulatory loop requires
571 PC, which is low in ER/Golgi membranes in *sams-1* and *sbp-1* RNAi animals. DAG kinases,
572 which could be stimulated by changes in DAGs in the *sbp-1* or *sams-1(RNAi)* animals, can also
573 affect ARF activity and trafficking (*89*). Finally, Protein Kinase D has an important role in
574 maintaining Golgi structure, and its ortholog has been linked to immunity in *C. elegans* (*90*, *91*).
575 However, DAG kinase or PKD (Protein Kinase D) loss failed to activate the p*sysm-1::GFP*
576 reporter in our RNAi screen, suggesting they could be important in other regulatory contexts.
577 While the lipidomic changes in *sbp-1* and *sams-1* animals are broad and individual lipids could
578 act through multiple independent mechanisms, our results show that decreasing PC is sufficient
579 to limit ARF-1 function (*25*) and activate ILG expression in the absence of pathogen.
580

581 Stress-responsive genes, such as ILGs, may contain several classes of factors with distinct
582 functions. Many of the ILGs, for example, those in the STRESS RESPONSE: Pathogen:
583 unassigned WormCat categories (*27*, *28*), lack domains associated with AMP function. While
584 some could have antimicrobial properties with distinct motifs, the activation of these genes
585 through intrinsic stress in the Golgi prompted us to ask if others acted to support secretory
586 function. Our data showing that reduction of *hpo-6, irg-2* and *irg-8* increased aggregation and
587 pooling of a secreted reporter in control and *sbp-1(ep79)* backgrounds suggests they could
588 protect or support secretory function occurring after broad disruption in membrane lipids or after
589 pathogen exposure occurs because both processes stress the trafficking system. Thus, some
590 ILGs may function generally a "multi-membrane" stress response encompassing the roles of both
591 the ER and the Golgi in trafficking. Taken together, these results illustrate mechanisms linking
592 lipid metabolism to genes activated in the immune response through effects on the secretory
593 system.
594
595

596 **Materials and Methods**

597 ***C. elegans* strains, RNAi constructs, and screening**.

598 N2 (wild type), p*sysm-1::GFP (*AU78*), myo-3*::GFP (GS1912), MANS::GFP (RT1315) and
599 OP50-1 were obtained from the *Caenorhabditis* Genetics Center. Exglo-1::ssGFP (GH639) was
600 a gift from Dr. Greg Hermann (Lewis and Clark University). *myo-3::ssGFP*;*sbp-*
601 *1(ep79)*(WAL510) was constructed in this study. CRISPR-tagged ARF-1, p*arf-1::ARF-*
602 *1::mCherry (knu418),* was obtained from the In Vivo Biosystems (COP1415) and then
603 outcrossed 3 times (WAL10). Imaging of MANS::GFP was done from a strain also harboring a
604 CRISPR tagged warf-1::RFP (ker4) (WAL12). (*cld-1*/C32H11.6::GFP was constructed by
605 SUNY Biotech using CRISPR (PHX2081(*sybIS7080*)). Normal growth media (NGM) was used
606 unless otherwise noted. For RNAi, gravid adults were bleached onto NGM plates supplemented
607 with ampicillin, tetracycline, and 6mM IPTG and 10X concentrated bacterial cultures. *C.*
608 *elegans* were allowed to develop until the young adult stage before harvesting. Because of larval
609 arrest, *copa-1* RNAi bacteria were diluted 1:10 in control RNAi bacteria before plating. For the
610 RNAi screen of *psysm-1*::GFP, L1 larvae were plated into 96 well plates spotted with RNAi
611 bacteria, and L4/young adults were scored from -3 to +3 with 0 as no change in 4 independent
612 replicates on a Zeiss GFP dissecting scope with an Axiocam camera. Candidates that were
613 positive in ¾ replicates were tested an additional four times, imaging 3 sets of 10 animals per
614 RNAi. Images quantitation is described below. For RNAi screen of *myo-3*::ssGFP and *myo-*
615 *3*::ssGFP; *sbp-1(ep79)*, 4 independent replicates were subjected to RNAi, placed in channeled
616 agarose pads and confocal images were collected on a Leica SP6.

617

618 **Cell culture and siRNA transfection**

619 HepG2 cells (ATCC, HB-8065) were grown in Minimum Essential Medium (Invitrogen) plus
620 10% FBS (Invitrogen), Glutamine (Invitrogen), and Sodium Pyruvate (Invitrogen). siRNA
621 oligonucleotides transfections were done for 48 hours using Lipofectamine RNAiMAX
622 Transfection Reagent (Invitrogen, 13778100), and cells were held for 16 hours in 1%
623 Lipoprotein Deficient Serum (LDS) (Biomedical Technologies, BT907) and 25 µg/ml ALLN
624 (Calbiochem) for 30 min prior to harvesting.
625
626 **Immunoblotting:**
627 **HepG2 cells:** Syringe passage was used to lyse cells in High Salt RIPA (50 mM Tris, pH 7.4;
628 400 mM NaCl; 0.1% SDS; 0.5% NaDeoxycholate; 1% NP-40; 1 mM DTT, 2.5 µg/mL ALLN,
629 Complete protease inhibitors (Roche). Invitrogen NuPage gels (4- 12%) were used for protein
630 separation before transfer to nitrocellulose. Blots were probed with antibodies to phosphorylated
631 p38 MAP Kinase, total p38, and STAT1 were used as a control. Immune complexes were
632 visualized with Luminol Reagent (Millipore). Densitometry was performed by scanning the
633 film, then analysis of pixel intensity with ImageJ software. Graphs show the average of at least
634 three independent experiments with control values normalized to one.
635
636 ***C. elegans:*** Young adult animals were lysed by sonication in High Salt RIPA, and
637 immunoblotting was performed as above.
638
639 **Microscopy and Image quantitation**
640 ARF-1::mCherry, MANS-1::GFP and ssGFP images were acquired on a Leica SPE confocal,
641 and projections of confocal slices were produced. All images were taken at identical gain

642 settings within experimental sets, and Adobe Photoshop was used for corrections to levels across
643 experimental sets. Image quantitation of GFP fluorescence was done using FIJI/ImageJ2.
644 Briefly, each photo was processed individually, beginning by splitting the image into three color
645 channels (Red/Green/Blue) and choosing the green channel for analysis. This image was then
646 converted to an 8-bit grey image and processed using the function "Enhance Local Contrast
647 (CLAHE)" (Blocksize: 250, Histogram bins: 256, Max Slope: 5.00, Mask: none, Fast (less
648 accurate): no (unchecked)). Using the circle selection tool, four sections (w: 55 h: 25) of the
649 brightest areas across each worm's intestine were selected from this processed image and
650 measured for intensity (integrated intensity). One additional section was taken from beside each
651 worm to account for background fluorescence. The background reading was subtracted from
652 each individual intestinal reading, then the four corrected readings were added to get a sum of
653 fluorescent intensity. Imaging of C32H11.9/*cld-1*::GFP was performed on a W1
654 Yokogawa spinning disk confocal microscope equipped with a Photometrics Prime BSI Express
655 sCMOS camera. Quantitation was performed with Nikon Imaging System software. Statistical
656 tests performed include Normality and Lognormality tests (Anderson-Darling, D'Agostino &
657 Pearson, Shapiro-Wilk, Kolmogorov-Smirnov) and Mann-Whitney tests.
658
659 **Lipidomics**
660 *C. elegans* total and microsomal lipidomics, including fractionation protocols, were performed
661 at the Whitehead Metabolomics core as in Smulan et al. 2016. Statistical analysis was
662 performed in Graphpad prism.
663
664 **Gene expression analysis**

665 Lysis of young adult *C. elegans* was performed in 0.5% SDS, 5% β-ME, 10 mM EDTA, 10 mM
666 Tris-HCl ph7.4, 0.5 mg/ml Proteinase K, before purification of RNA by TRI-Reagent (Sigma).
667 cDNA was produced with Transcriptor First-strand cDNA kits (Roche), and RT-PCR was
668 performed using Kappa SYBR Green 2X Mastermix.
669
670 RNA for sequencing was purified using RNAeasy columns (Qiagen). RNA sequencing
671 (including library construction was performed by BGI (Hong Kong). Reads were analyzed
672 through the Dolphin analysis platform (https://dolphin.umassmed.edu/), using DeSeq to identify
673 differentially expressed genes (*92*). Gene set enrichment was performed using WormCat
674 (www.wormcat.com) (*27*, *28*).
675
676

Acknowledgments

We would like acknowledge Drs. Seung-Jae Lee, Sujeong Kwon (Korea Advanced Institute of Science and Technology) for providing the *lpin-1* RNA seq data. In addition, Dr. Greg Hermann provided the *glo-1*::ssGFP strain (GH639). We would also like to thank Drs. Seung-Jae Lee, Emily Troemel (USD), Cole Haynes (UMASS Chan School of Medicine), Alexandra Byrne (UMASS Chan School of Medicine) and members of the Walker lab for comments on the manuscript in addition to Dr. Marian Walhout (UMASS Chan School of Medicine) for helpful discussion. We would like to acknowledge Wei Ding for technical support and Caroline Lewis (MIT) for metabolomics screening at the Whitehead Metabolomics core. We also thank Life Science Editors and Dr. Sabbi Lall for manuscript editing. Funding was from the NIA at the NIH: R01AG053355, R56AG068670 and R01AG068670. Some strains were provided by the CGC, which is funded by the NIH Office of Research Infrastructure Programs (P40 OD010440).

Author Contributions

Conceptualization; AKW, MJF, CMW, LJS

Verification: AKW, , MJF, CMW, LJS

Formal Analysis: AKW, MJF, CMW, LJS, DML

Investigation: AKW, MJF,CMW, LJS, DL, MF

Resources: AKW

Data Curation: AKW

Writing: AKW

Writing/Editing: AKW, MJF, CMW, DSL, LJS

Visualization: AKW

Supervision: AKW

Funding: AKW

Declaration of Interests

The authors declare no competing interests.

Data and materials availability:

All data are available in the main text or the supplementary materials will be shared. GEO submission of RNA seq data is in progress.

720 **References**

721

722 1. K. E. Wellen, C. B. Thompson, A two-way street: reciprocal regulation of metabolism and
723 signalling *Mol Cell*, (2010).

724 2. J. Aramburu, M. C. Ortells, S. Tejedor, M. Buxadé, C. López-Rodríguez, Transcriptional
725 regulation of the stress response by mTOR. *Sci Signal*. 7, re2–re2 (2014).

726 3. H. G. Son, O. Altintas, E. J. E. Kim, S. Kwon, S. V. Lee, Age-dependent changes and
727 biomarkers of aging in *Caenorhabditis elegans*. *Aging Cell*. 18, e12853 (2019).

728 4. K. Halbleib, K. Pesek, R. Covino, H. F. Hofbauer, D. Wunnicke, I. Hänelt, G. Hummer, R.
729 Ernst, Activation of the Unfolded Protein Response by Lipid Bilayer Stres. *Mol Cell*, (2017).

730 5. M. A. Gianfrancesco, N. Paquot, J. Piette, S. Legrand-Poels, Lipid bilayer stress in obesity-
731 linked inflammatory and metabolic disorders. *Biochem Pharmacol*. 153, 168–183 (2018).

732 6. J. H. Koh, L. Wang, C. Beaudoin-Chabot, G. Thibault, Lipid bilayer stress-activated IRE-1
733 modulates autophagy during endoplasmic reticulum stress. *J Cell Sci*. 131, jcs217992 (2018).

734 7. T. Radanović, J. Reinhard, S. Ballweg, K. Pesek, R. Ernst, An Emerging Group of Membrane
735 Property Sensors Controls the Physical State of Organellar Membranes to Maintain Their
736 Identity. *Bioessays*. 40, 1700250 (2018).

737 8. G. S. Hotamisligil, R. J. Davis, Cell Signaling and Stress Responses. *Csh Perspect Biol*. 8,
738 a006072 (2016).

739 9. W. Ding, L. J. Smulan, N. S. Hou, S. Taubert, J. L. Watts, A. K. Walker, s-
740 Adenosylmethionine Levels Govern Innate Immunity through Distinct Methylation-Dependent
741 Pathways *Cell Metab*, (2015).

742 10. A. K. Walker, R. L. Jacobs, J. L. Watts, V. Rottiers, K. Jiang, D. M. Finnegan, T. Shioda, M.
743 Hansen, F. Yang, L. J. Niebergall, D. E. Vance, M. Tzoneva, A. C. Hart, A. M. Näär, A
744 Conserved SREBP-1/Phosphatidylcholine Feedback Circuit Regulates Lipogenesis in
745 Metazoans. *Cell*, (2011).

746 11. T. L. Dunbar, Z. Yan, K. M. Balla, M. G. Smelkinson, E. R. Troemel, *C. elegans* detects
747 pathogen-induced translational inhibition to activate immune signaling. *Cell Host Microbe*,
748 (2012).

749 12. J. D. Horton, J. L. GOLDSTEIN, M. S. BROWN, SREBPs: Transcriptional Mediators of
750 Lipid Homeostasis. *Cold Spring Harb Sym*. 67, 491–498 (2002).

751 13. R. M. McKay, J. P. McKay, L. Avery, J. M. Graff, C. elegans A Model for Exploring the
752 Genetics of Fat Storage. *Dev Cell*. 4, 131–142 (2003).

753 14. S. Wu, A. M. Näär, SREBP1-dependent de novo fatty acid synthesis gene expression is
754 elevated in malignant melanoma and represents a cellular survival trait. *Sci Rep-uk*. 9, 10369
755 (2019).

756 15. N. Ho, W. S. Yap, J. Xu, H. Wu, J. H. Koh, W. W. B. Goh, B. George, S. C. Chong, S.
757 Taubert, G. Thibault, Stress sensor Ire1 deploys a divergent transcriptional program in response
758 to lipid bilayer stress. *J Cell Biol*. 219 (2020), doi:10.1083/jcb.201909165.

759 16. Y. Jung, S. Kwon, S. Ham, D. Lee, H. H. Park, Y. Yamaoka, D. Jeong, M. Artan, O.
760 Altintas, S. Park, W. Hwang, Y. Lee, H. G. Son, S. W. A. An, E. J. E. Kim, M. Seo, S. V. Lee,
761 *Caenorhabditis elegans* Lipin 1 moderates the lifespan-shortening effects of dietary glucose by
762 maintaining ω-6 polyunsaturated fatty acids. *Aging Cell*. 19 (2020), doi:10.1111/acel.13150.

763 17. J. D. Nhan, C. D. Turner, S. M. Anderson, C.-A. Yen, H. M. Dalton, H. K. Cheesman, D. L.
764 Ruter, N. U. Naresh, C. M. Haynes, A. A. Soukas, R. Pukkila-Worley, S. P. Curran, Redirection
765 of SKN-1 abates the negative metabolic outcomes of a perceived pathogen infection. *Proc*
766 *National Acad Sci*. 116, 22322–22330 (2019).

767 18. Z. Wu, M. Isik, N. Moroz, M. J. Steinbaugh, P. Zhang, T. K. Blackwell, Dietary Restriction
768 Extends Lifespan through Metabolic Regulation of Innate Immunity. *Cell Metab*. 29, 1192-
769 1205.e8 (2019).

770 19. I. Engelmann, A. Griffon, L. Tichit, F. Montañana-Sanchis, G. Wang, V. Reinke, R. H.
771 Waterston, L. W. Hillier, J. J. Ewbank, A Comprehensive Analysis of Gene Expression Changes
772 Provoked by Bacterial and Fungal Infection in C. elegans. *Plos One*. 6, e19055 (2011).

773 20. G. V. Mallo, C. L. Kurz, C. Couillault, N. Pujol, S. Granjeaud, Y. Kohara, J. J. Ewbank,
774 Inducible Antibacterial Defense System in *C. elegans*. *Curr Biol*. 12, 1209–1214 (2002).

775 21. M. Fletcher, E. J. Tillman, V. L. Butty, S. S. Levine, D. H. Kim, Global transcriptional
776 regulation of innate immunity by ATF-7 in *C. elegans*. *Plos Genet*. 15, e1007830 (2019).

777 22. E. R. Troemel, S. W. Chu, V. Reinke, S. S. Lee, F. M. Ausubel, D. H. Kim, p38 MAPK
778 regulates expression of immune response genes and contributes to longevity in *C. elegans*. *Plos*
779 *Genet*. 2, e183 (2006).

780 23. K. A. Estes, T. L. Dunbar, J. R. Powell, F. M. Ausubel, E. R. Troemel, bZIP transcription
781 factor *zip-2* mediates an early response to Pseudomonas aeruginosa infection in *Caenorhabditis*
782 *elegans*. *Proc National Acad Sci*, (2010).

783 24. R. P. Shivers, T. Kooistra, S. W. Chu, D. J. Pagano, D. H. Kim, Tissue-Specific Activities of
784 an Immune Signaling Module Regulate Physiological Responses to Pathogenic and Nutritional
785 Bacteria in *C. elegans*. *Cell Host Microbe*. 6, 321–330 (2009).

786 25. L. J. Smulan, W. Ding, E. Freinkman, S. Gujja, Y. J. K. Edwards, A. K. Walker, Cholesterol-
787 Independent SREBP-1 Maturation Is Linked to ARF1 Inactivation. *Cell Reports*, (2016).

788 26. N. Zmora, S. Bashiardes, M. Levy, E. Elinav, The Role of the Immune System in Metabolic
789 Health and Disease. *Cell Metab*. 25, 506–521 (2017).

790 27. A. D. Holdorf, D. P. Higgins, A. C. Hart, P. R. Boag, G. J. Pazour, A. J. M. Walhout, A. K.
791 Walker, WormCat: An Online Tool for Annotation and Visualization of *Caenorhabditis elegans*
792 Genome-Scale Data. *Genetics*, (2019).

793 28. D. P. Higgins, C. M. Weisman, D. S. Lui, F. A. D'Agostino, A. K. Walker, Defining
794 characteristics and conservation of poorly annotated genes in *Caenorhabditis elegans* using
795 WormCat 2.0. *Genetics* (2022), doi:10.1093/genetics/iyac085.

796 29. W. Ding, D. P. Higgins, D. K. Yadav, A. A. Godbole, R. Pukkila-Worley, A. K. Walker,
797 Stress-responsive and metabolic gene regulation are altered in low S-adenosylmethionine. *Plos*
798 *Genet*. 14, e1007812 (2018).

799 30. S. Taubert, M. R. V. Gilst, M. Hansen, K. R. Yamamoto, A Mediator subunit, MDT-15,
800 integrates regulation of fatty acid metabolism by NHR-49-dependent and -independent pathways
801 in *C. elegans*. *Gene Dev*. 20, 1137–1149 (2006).

802 31. G. Y. S. Goh, J. J. Winter, F. Bhanshali, K. R. S. Doering, R. Lai, K. Lee, E. A. Veal, S.
803 Taubert, NHR-49/HNF4 integrates regulation of fatty acid metabolism with a protective
804 transcriptional response to oxidative stress and fasting. *Aging Cell*. 17, e12743 (2018).

805 32. M. L. Ladage, S. D. King, D. J. Burks, D. L. Quan, A. M. Garcia, R. K. Azad, P. A. Padilla,
806 Glucose or Altered Ceramide Biosynthesis Mediate Oxygen Deprivation Sensitivity Through
807 Novel Pathways Revealed by Transcriptome Analysis in *Caenorhabditis elegans*. *G3 Genes*
808 *Genomes Genetics*, (2016).

809 33. Y. J. Liu, G. E. Janssens, R. L. McIntyre, M. Molenaars, R. Kamble, A. W. Gao, A.
810 Jongejan, M. van Weeghel, A. W. MacInnes, R. H. Houtkooper, Glycine promotes longevity in
811 *Caenorhabditis elegans* in a methionine cycle-dependent fashion. *Plos Genet*. 15, e1007633
812 (2019).

813 34. N. D. Peterson, J. D. Icso, J. E. Salisbury, T. Rodríguez, P. R. Thompson, R. Pukkila-
814 Worley, Pathogen infection and cholesterol deficiency activate the *C. elegans* p38 immune
815 pathway through a TIR-1/SARM1 phase transition. *Elife*. 11, e74206 (2022).

816 35. D. P. Higgins, C. M. Weisman, D. S. Lui, F. A. D'Agostino, A. K. Walker, WormCat 2.0
817 defines characteristics and conservation of poorly annotated genes in *Caenorhabditis elegans*.
818 *Genetics* (2022), doi:10.1093/genetics/iyac085.

819 36. X. Shen, R. E. Ellis, K. Sakaki, R. J. Kaufman, Genetic Interactions Due to Constitutive and
820 Inducible Gene Regulation Mediated by the Unfolded Protein Response in C. elegans. *Plos*
821 *Genet*. 1, e37 (2005).

822 37. F. Yang, B. W. Vought, J. S. Satterlee, A. K. Walker, Z.-Y. J. Sun, J. L. Watts, R.
823 DeBeaumont, R. M. Saito, S. G. Hyberts, S. Yang, C. Macol, L. Iyer, R. Tjian, S. van den
824 Heuvel, A. C. Hart, G. Wagner, A. M. Näär, *Nature* (2006).

825 38. J. C. M. Holthuis, A. K. Menon, *Nature*, Lipid landscapes and pipelines in membrane
826 homeostasis (2014).

827 39. D. Jeong, D. Lee, S. Hwang, Y. Lee, J. Lee, M. Seo, W. Hwang, K. Seo, A. B. Hwang, M.
828 Artan, H. G. Son, J. Jo, H. Baek, Y. M. Oh, Y. Ryu, H. Kim, C. M. Ha, J. Yoo, S. V. Lee,
829 Mitochondrial chaperone HSP-60 regulates anti-bacterial immunity via p38 MAP kinase
830 signaling. *Embo J*. 36, 1046–1065 (2017).

831 40. C. L. Pender, H. R. Horvitz, Hypoxia-inducible factor cell non-autonomously regulates C.
832 elegans stress responses and behavior via a nuclear receptor. *Elife*. 7, e36828 (2018).

833 41. J. L. Watts, J. Browse, Genetic dissection of polyunsaturated fatty acid synthesis in
834 Caenorhabditis elegans. *Proc National Acad Sci*, (2006).

835 42. M. Ruiz, R. Bodhicharla, E. Svensk, R. Devkota, K. Busayavalasa, H. Palmgren, M.
836 Ståhlman, J. Boren, M. Pilon, Membrane fluidity is regulated by the C. elegans transmembrane
837 protein FLD-1 and its human homologs TLCD1/2. *Elife*. 7, 1309 (2018).

838 43. R. Bodhicharla, R. Devkota, M. Ruiz, M. Pilon, *Genetics*, Membrane Fluidity Is Regulated
839 Cell Non-autonomously by Caenorhabditis elegans PAQR-2 and Its Mammalian Homolog
840 AdipoR2 (2018).

841 44. N. Ho, C. Xu, G. Thibault, From the unfolded protein response to metabolic diseases – lipids
842 under the spotlight. *J Cell Sci*. 131, jcs199307 (2018).

843 45. A. Spang, ARF1 regulatory factors and COPI vesicle formation. *Curr Opin Cell Biol*. 14,
844 423–427 (2002).

845 46. A. G. Fraser, R. S. Kamath, P. Zipperlen, M. Martinez-Campos, M. Sohrmann, J. Ahringer,
846 Functional genomic analysis of *C. elegans* chromosome I by systematic RNA interference.
847 *Nature*. 408, 325–330 (2000).

848 47. M. A. Gustafson, J. C. Fromme, Regulation of Arf activation occurs via distinct mechanisms
849 at early and late Golgi compartments. *Mol Biol Cell*, (2017).

850 48. J. R. Broekhuis, S. Rademakers, J. Burghoorn, G. Jansen, SQL-1, homologue of the Golgi
851 protein GMAP210, modulates intraflagellar transport in *C. elegans*. *J Cell Sci*. 126, 1785–1795
852 (2013).

853 49. C. C.-H. Chen, P. J. Schweinsberg, S. Vashist, D. P. Mareiniss, E. J. Lambie, B. D. Grant,
854 RAB-10 Is Required for Endocytic Recycling in the Caenorhabditis elegans Intestine *Mol Biol*
855 *Cell*, (2006).

856 50. M. M. Rolls, D. H. Hall, M. Victor, E. H. K. Stelzer, T. A. Rapoport, Targeting of Rough
857 Endoplasmic Reticulum Membrane Proteins and Ribosomes in Invertebrate Neurons. *Mol Biol*
858 *Cell*. 13, 1778–1791 (2002).

859 51. R. D. Klausner, J. G. Donaldson, J. Lippincott-Schwartz, Brefeldin A: insights into the
860 control of membrane traffic and organelle structure. *The Journal of cell biology*, 1992.

861 52. K. Sato, M. Sato, A. Audhya, K. Oegema, P. Schweinsberg, B. D. Grant, Dynamic
862 Regulation of Caveolin-1 Trafficking in the Germ Line and Embryo of Caenorhabditis elegans
863 *Mol Biol Cell*, (2006).

864 53. K. B. Ackema, U. Sauder, J. A. Solinger, A. Spang, The ArfGEF GBF-1 Is Required for ER
865 Structure, Secretion and Endocytic Transport in *C. elegans*. *Plos One*. 8, e67076 (2013).

866 54. I. D. Zelnik, A. E. Ventura, J. L. Kim, L. C. Silva, A. H. Futerman, The role of ceramide in
867 regulating endoplasmic reticulum function. *Biochimica Et Biophysica Acta Bba - Mol Cell*
868 *Biology Lipids* (2019), doi:10.1016/j.bbalip.2019.06.015.

869 55. G. Boncompain, A. V. Weigel, Transport and sorting in the Golgi complex: multiple
870 mechanisms sort diverse cargo. *Curr Opin Cell Biol*. 50, 94–101 (2018).

871 56. T. Taguchi, K. Mukai, Innate immunity signalling and membrane trafficking. *Curr Opin Cell*
872 *Biol*. 59, 1–7 (2019).

873 57. B. M. Gardner, D. Pincus, K. Gotthardt, C. M. Gallagher, P. Walter, Endoplasmic Reticulum
874 Stress Sensing in the Unfolded Protein Response. *Csh Perspect Biol*. 5, a013169 (2013).

875 58. T. Lamitina, E. Chevet, To UPR… and beyond!: A new role for a BiP/GRP78 protein in the
876 control of antimicrobial peptide expression in *C. elegans* epidermis. *Virulence*. 3, 238–240
877 (2012).

878 59. C. Couillault, P. Fourquet, M. Pophillat, J. J. Ewbank, A UPR-independent infection-specific
879 role for a BiP/GRP78 protein in the control of antimicrobial peptide expression in *C. elegans*
880 epidermis *Virulence*, 2012.

881 60. B. D. Grant, M. Sato, Intracellular trafficking. *Wormbook Online Rev C Elegans Biology*, 1–
882 9 (2006).

883 61. H. Fares, I. Greenwald, Genetic Analysis of Endocytosis in *Caenorhabditis elegan*s :
884 Coelomocyte Uptake Defective Mutants. *Genetics*. 159, 133–145 (2001).

885 62. B. Grant, D. Hirsh, Evidence that RME-1, a conserved *C. elegans* EH-domain protein,
886 functions in endocytic recycling *Mol Biol Cell*, (2001).

887 63. M. J. Steinbaugh, S. D. Narasimhan, S. Robida-Stubbs, L. E. M. Mazzeo, J. M. Dreyfuss, J.
888 M. Hourihan, P. Raghavan, T. N. Operaña, R. Esmaillie, T. K. Blackwell, Lipid-mediated
889 regulation of SKN-1/Nrf in response to germ cell absence. *Elife*. 4, 466 (2015).

890 64. J. Singh, A. Aballay, Endoplasmic Reticulum Stress Caused by Lipoprotein Accumulation
891 Suppresses Immunity against Bacterial Pathogens and Contributes to Immunosenescence. *Mbio*.
892 8, e00778-17 (2017).

893 65. Z. Balklava, N. D. Rathnakumar, S. Vashist, P. J. Schweinsberg, B. D. Grant, *Genetics*,
894 Genome-wide analysis identifies a general requirement for polarity proteins in endocytic traffic
895 (2016).

896 66. L. V. Rompay, C. Borghgraef, I. Beets, J. Caers, L. Temmerman, New genetic regulators
897 question relevance of abundant yolk protein production in *C. elegans Sci Rep-uk*, (2015).

898 67. C.-Y. Kao, F. C. O. Los, D. L. Huffman, S. Wachi, N. Kloft, M. Husmann, V. Karabrahimi,
899 J.-L. Schwartz, A. Bellier, C. Ha, Y. Sagong, H. Fan, P. Ghosh, M. Hsieh, C.-S. Hsu, L. Chen, R.
900 V. Aroian, Global Functional Analyses of Cellular Responses to Pore-Forming Toxins. *Plos*
901 *Pathog*. 7, e1001314 (2011).

902 68. W. Rao, R. E. Isaac, J. N. Keen, An analysis of the *Caenorhabditis elegans* lipid raft
903 proteome using geLC-MS/MS *J Proteomics*, (2011).

904 69. M. F. Perez, B. Lehner, Vitellogenins - Yolk Gene Function and Regulation in
905 *Caenorhabditis elegans*. *Front Physiol*. 10, 1067 (2019).

906 70. A. E. Carpenter, T. R. Jones, M. R. Lamprecht, C. Clarke, I. H. Kang, O. Friman, D. A.
907 Guertin, J. H. Chang, R. A. Lindquist, J. Moffat, P. Golland, D. M. Sabatini, CellProfiler: image
908 analysis software for identifying and quantifying cell phenotypes. *Genome Biol*. 7, R100 (2006).

909 71. G. J. Hermann, L. K. Schroeder, C. A. Hieb, A. M. Kershner, B. M. Rabbitts, P. Fonarev, B.
910 D. Grant, J. R. Priess, Genetic Analysis of Lysosomal Trafficking in *Caenorhabditis elegans*.
911 *Mol Biol Cell*. 16, 3273–3288 (2005).

912 72. A. Shaheen, Effect of the unfolded protein response on ER protein export: a potential new
913 mechanism to relieve ER stress. *Cell Stress Chaperones*. 23, 797–806 (2018).

914 73. C. E. Richardson, T. Kooistra, D. H. Kim, An essential role for XBP-1 in host protection
915 against immune activation in C. elegans. *Nature*, (2010).

916 74. J. J. Ewbank, O. Zugasti, *C. elegans*: model host and tool for antimicrobial drug discovery.
917 *Dis Model Mech*. 4, 300–304 (2011).

918 75. R. Medzhitov, Recognition of microorganisms and activation of the immune response.
919 *Nature*. 449, 819–826 (2007).

920 76. B. A. Martínez, R. G. Hoyle, S. Yeudall, M. E. Granade, T. E. Harris, J. D. Castle, N.
921 Leitinger, M. L. Bland, Innate immune signaling in *Drosophila* shifts anabolic lipid metabolism
922 from triglyceride storage to phospholipid synthesis to support immune function. *Plos Genet*. 16,
923 e1009192 (2020).

924 77. M. Safra, S. Ben-Hamo, C. Kenyon, S. Henis-Korenblit, The *ire-1* ER stress-response
925 pathway is required for normal secretory-protein metabolism in *C. elegans*. *J Cell Sci*. 126,
926 4136–4146 (2013).

927 78. D. L. McEwan, N. V. Kirienko, F. M. Ausubel, *Cell Host Microbe*, (2010).

928 79. E. J. Tillman, C. E. Richardson, D. J. Cattie, K. C. Reddy, N. J. Lehrbach, R. Droste, G.
929 Ruvkun, D. H. Kim, *Genetics*, (2018).

930 80. D.-E. Jeong, Y. Lee, S. Ham, D. Lee, S. Kwon, H.-E. H. Park, S.-Y. Hwang, J.-Y. Yoo, T.-Y.
931 Roh, S.-J. V. Lee, Inhibition of the oligosaccharyl transferase in *Caenorhabditis elegans* that
932 compromises ER proteostasis suppresses p38-dependent protection against pathogenic bacteria.
933 *Plos Genet*. 16, e1008617 (2020).

934 81. N. G. Bednarska, B. W. Wren, S. J. Willcocks, The importance of the glycosylation of
935 antimicrobial peptides: natural and synthetic approaches. *Drug Discov Today*. 22, 919–926
936 (2017).

937 82. K. Dierking, W. Yang, H. Schulenburg, Antimicrobial effectors in the nematode
938 *Caenorhabditis elegans*: an outgroup to the Arthropoda. *Philosophical Transactions Royal Soc B*
939 *Biological Sci*. 371, 20150299 (2016).

940 83. E. de Nadal, G. Ammerer, F. Posas, Controlling gene expression in response to stress. *Nat*
941 *Rev Genet*. 12, 833–845 (2011).

942 84. C. E. Machamer, The Golgi complex in stress and death. *Front Neurosci-switz*. 9, 421
943 (2015).

944 85. J. H. Reiling, A. J. Olive, S. Sanyal, J. E. Carette, T. R. Brummelkamp, H. L. Ploegh, M. N.
945 Starnbach, D. M. Sabatini, *Nat Cell Biol*, (2013).

946 86. J. G. Donaldson, C. L. Jackson, *Nat Rev Mol Cell Bio*, (2011).

947 87. C. Riebeling, A. J. Morris, D. Shields, *Biochimica Et Biophysica Acta Bba - Mol Cell*
948 *Biology Lipids*, (2009).

949 88. M. McDermott, M. J. O. Wakelam, A. J. Morris, Phospholipase D. *Biochem Cell Biol*. 82,
950 225–253 (2004).

951 89. R. P. H. Huijbregts, L. Topalof, V. A. Bankaitis, Lipid Metabolism and Regulation of
952 Membrane Trafficking. *Traffic*. 1, 195–202 (2000).

953 90. M. Ren, H. Feng, Y. Fu, M. Land, C. S. Rubin, Protein Kinase D Is an Essential Regulator of
954 *C. elegans* Innate Immunity. *Immunity*. 30, 521–532 (2009).

955 91. V. Malhotra, F. Campelo, *Csh Perspect Biol*, (2011).

956 92. O. Yukselen, O. Turkyilmaz, A. R. Ozturk, M. Garber, A. Kucukural, DolphinNext: a
957 distributed data processing platform for high throughput genomics. *Bmc Genomics*. 21, 310
958 (2020).

959